Journal of Quantitative Spectroscopy & Radiative Transfer 112 (2011) 2639–2660

Contents lists available at ScienceDirect

Journal of Quantitative Spectroscopy & Radiative Transfer

journal homepage: www.elsevier.com/locate/jqsrt

Review

Radiation transfer in photobiological carbon dioxide fixation and fuel production by microalgae

Laurent Pilon [a,*], Halil Berberoğlu [b,1], Razmig Kandilian [a]

[a] Mechanical and Aerospace Engineering Department, Henry Samueli School of Engineering and Applied Science, University of California, Los Angeles, 420 Westwood Plaza, Eng. IV 37-132, Los Angeles, CA 9095-1597, USA
[b] Mechanical Engineering Department, Cockrell School of Engineering, The University of Texas at Austin, 204 E. Dean Keeton Street, Austin, TX 78705, USA

ARTICLE INFO

Article history:
Received 26 April 2011
Received in revised form
18 July 2011
Accepted 20 July 2011
Available online 29 July 2011

Keywords:
Photobioreactor
Scattering
Chlorophyll
Ocean optics
Hydrogen
Lipid production
Biofuels
Cyanobacteria
Light transfer

ABSTRACT

Solar radiation is the energy source driving the metabolic activity of microorganisms able to photobiologically fixate carbon dioxide and convert solar energy into biofuels. Thus, careful radiation transfer analysis must be conducted in order to design and operate efficient photobioreactors. This review paper first introduces light harvesting mechanisms used by microorganisms as well as photosynthesis and photobiological fuel production. It then provides a thorough and critical review of both experimental and modeling efforts focusing on radiation transfer in microalgae suspension. Experimental methods to determine the radiation characteristics of microalgae are presented. Methods for solving the radiation transfer equation in photobioreactors with or without bubbles are also discussed. Sample measurements and numerical solutions are provided. Finally, novel strategies for achieving optimum light delivery and maximizing sunlight utilization in photobioreactors are discussed including genetic engineering of microorganisms with truncated chlorophyll antenna.

Contents

* Corresponding author. Tel.: +1 310 206 5598; fax: +1 310 206 2302.
E-mail addresses: pilon@seas.ucla.edu (L. Pilon), berberoglu@mail.utexas.edu (H. Berberoğlu).
URL: http://www.seas.ucla.edu/~pilon (L. Pilon).
[1] Tel.: +1 512 232 8459; fax: +1 512 471 1045.

0022-4073/$ - see front matter © 2011 Elsevier Ltd. All rights reserved.
doi:10.1016/j.jqsrt.2011.07.004

1. Introduction

1.1. World energy challenges

Industrial and developing nations are facing an unprecedented combination of economic, environmental, and political challenges. First, they face the formidable challenge to meet ever expanding energy needs without further impacting the climate and the environment. Second, the continued population growth in developing countries and the emergence of a global economy are creating unprecedented stress on the resources of the Earth. Emerging countries are claiming access to the same standard of living as that of industrial nations, resulting in large needs for energy sources, fast and reliable transportation systems, and industrial equipment. From the standpoint of international security, energy issues include the potential for conflict over access to remaining supplies of inexpensive fossil fuels, which are often concentrated in politically unstable regions.

Currently, fossil fuels supply more than 81% of the world's energy needs estimated at about 137 PWh/year (1 PW = 1^{15} W) or 493 EJ/year (1 EJ = 10^{18} J) [1]. Oil meets more than 92% of the world transportation energy needs [1]. However, its production is expected to peak between 2000 and 2050 after which its production will enter a terminal decline [2]. Simultaneously, the world energy consumption is expected to grow by 50% between 2005 and 2030 [2]. Thus, the end of easily accessible and inexpensive oil is approaching.

Moreover, intensive use of fossil fuels increases the concentration of carbon dioxide (CO_2) in the atmosphere and contributes to global climate changes [3]. For example, 71.4% of the electricity consumed in the United States is generated from fossil fuel, mainly coal and natural gas [4]. In 2006, electricity generation alone contributed to 33% of the total CO_2 emissions of the United States, which in turn represented approximately 23% of the total global CO_2 emissions [2].

Flue gases from fossil fuel power plants consist of 4–14 vol% of CO_2 and up to 200 ppm of NO_x and SO_x, depending on the type of fuel and on the combustion process [5]. Overall, the concentration of CO_2 in the atmosphere in 2006 varied between 360 and 390 part per million by volume (ppmv) during that year and continue to increase [6]. It is predicted that CO_2 levels above 450 ppm in the atmosphere will have severe impact on sea levels, global climate patterns, and survival of many species [3]. Consequently, growing energy needs calls for greater reliance on a combination of fossil fuel-free renewable energy sources and on new technologies for capturing and converting CO_2.

1.2. Solar radiation

Seen from the earth, the sun is approximately a disk of radius 6.96×10^8 m at an average distance of 1.496×10^{11} m and viewed with a solid angle of 6.8×10^{-5} sr. The Sun is often approximated as a blackbody at 5800 K emitting according to Planck's law [7]. The solar constant is defined as the total energy incident per unit time per unit surface area at the outer surface of Earth's atmosphere and oriented perpendicular to the sun's rays; it is estimated to be 1367 W/m^2 [7,8]. As the solar radiation travels through the Earth's atmosphere it is absorbed by atmospheric gases (e.g., CO_2, H_2O) and scattered by gas

molecules and larger aerosol particles, ice crystals, or water droplets. Once it reaches the Earth's surface most of the ultraviolet (UV) component has been absorbed by oxygen and ozone molecules. Attenuation in the visible part of the electromagnetic spectrum is mainly due to Rayleigh scattering by small gas molecules such as oxygen (O_2) and water vapor (H_2O). In the near-infrared part of the spectrum, the main absorber is water vapor with contributions from CO_2. Other minor absorbers include nitrous oxide (N_2O), carbon monoxide (CO), and methane (CH_4) [7]. The solar radiation reaching the Earth's atmosphere consists of 6.4% of UV radiation ($\lambda < 380$ nm), 48% of visible light ($380 \leq \lambda \leq 780$ nm), and 45.6% of infrared radiation ($\lambda > 780$ nm) [8]. Overall, the sun delivers 1.73×10^{17} W or 6.38×10^{19} Wh/year on the surface of the atmosphere [8]. This significantly exceeds the 2006 world energy consumption rate of 1.56×10^{13} W or an annual total energy of 1.37×10^{17} Wh/year [1].

The solar spectrum incident on earth depends on the latitude and altitude. The ASTM G173-03 standard [9] provides reference terrestrial solar spectral irradiance (within 2π steradian field of view) for wavelength ranging from 280 to 4000 nm and averaged over one year and over the 48 contiguous states of the continental United States under atmospheric conditions corresponding to the United States standard atmosphere [10]. Fig. 1 shows (i) the extraterrestrial spectral irradiance [9], (ii) the direct normal spectral irradiance at sea level with an air mass of 1.5, and (iii) the hemispherical (or global) spectral irradiance on a inclined plane at sea level, tilted at 37° toward the equator and facing the sun. The data were produced using the Simple Model for Atmospheric Transmission of Sunshine (SMARTS2 version 2.9.2) [11]. Absorption due to atmospheric O_3, O_2, CO_2, and H_2O is apparent in the direct normal irradiance. Moreover, Fig. 2 shows the amount of daily solar irradiance in hours incident on an optimally tilted surface during the worst month of the year based on worldwide solar insolation data [12]. The figure indicates that the most promising regions for harvesting solar energy are the southwest United States, northern Mexico, the Andes, northern and southern Africa and the Middle East, as well as Australia. Other regions with favorable conditions include southern Europe, southern China, South East Asia, Brazil, and most of Africa. Note that many of these regions have limited freshwater resources.

1.3. Microbial photosynthesis

Most photosynthetic microorganisms use water as their electron source, sunlight as their energy source, and CO_2 as their carbon source. In turn they produce oxygen and carbohydrates, protein, and lipids contained within the cells as illustrated in Fig. 3. They are typically more efficient than higher plants (e.g., trees or sugar cane) at converting solar energy into biomass [13] thanks to their simple cellular structure and the readily available supply of CO_2 and various nutrients dissolved in water. In fact, microalgae can produce 30 times more oil than terrestrial oilseed crops for a given surface area [14]. Moreover, microalgae require 140–200 kg of water per kilogram of C fixed compared with more than 550 kg of water per kg of CO_2 fixed by trees [15]. Unlike for trees, water for microalgae can be low quality (waste water) and even high salinity water both unsuitable for agriculture use or human consumption [15]. Note also that some species can grow in high concentration thus reducing water needs. Thus, cultivation of these microorganisms offer a sustainable method for carbon dioxide capture and storage [16–19] suitable in semi-arid or arid lands without competing with

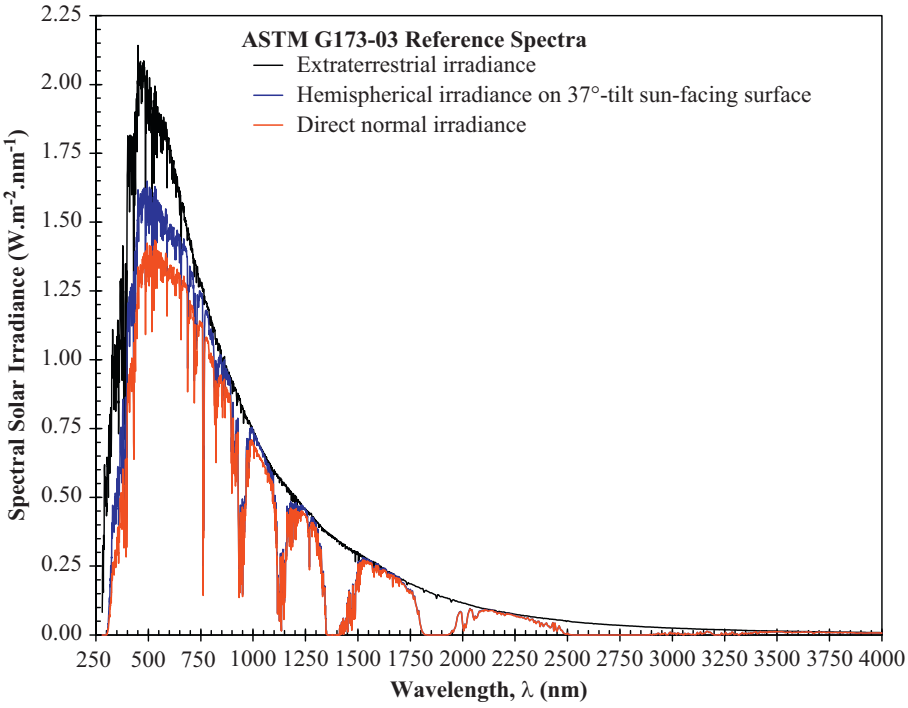

Fig. 1. Averaged daily extraterrestrial solar irradiance and ASTM G173-03 (direct and hemispherical, 37° sun-facing tilted) sea level irradiance in W/m^2 nm [9].

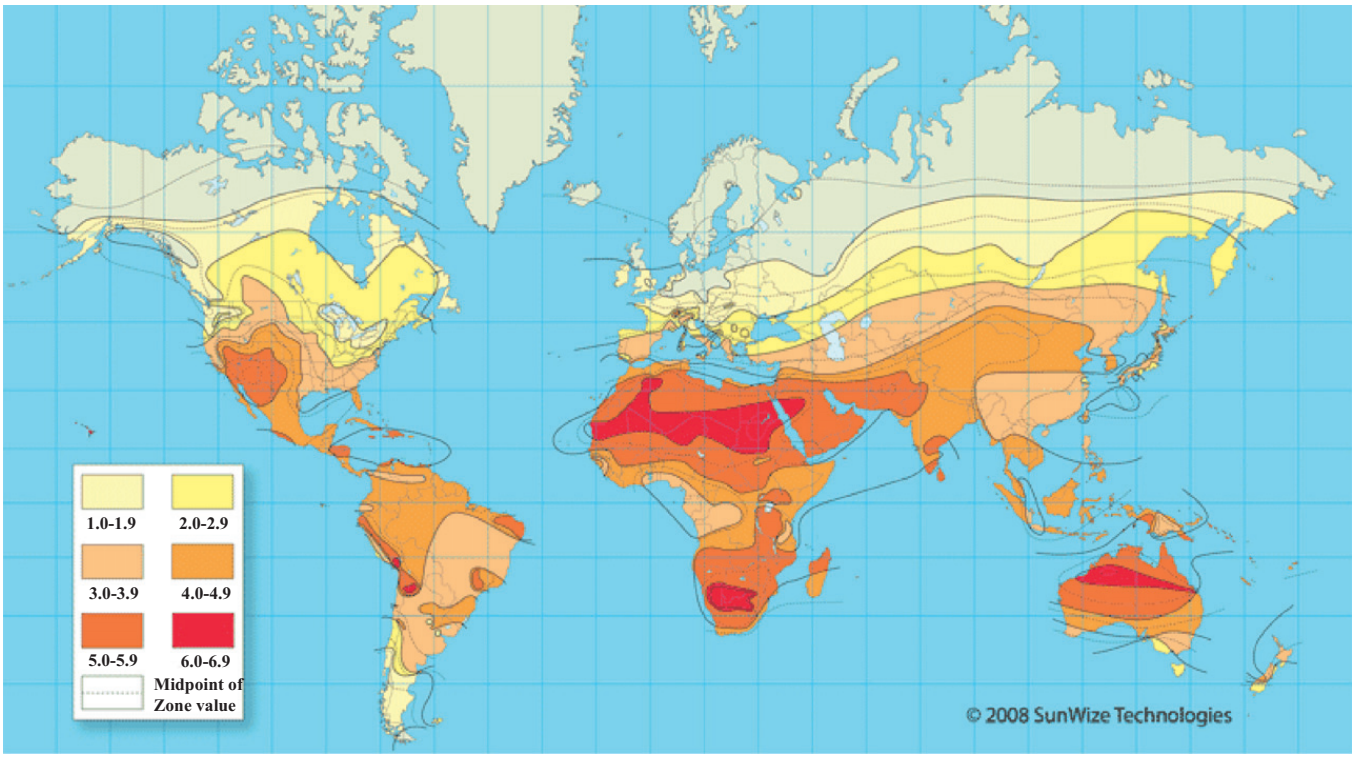

Fig. 2. Averaged daily local solar irradiance on an optimally tilted surface during the worst month of the year (units are in kWh/m^2/day). Used by permission. All rights reserved. © 2009 SunWize Technologies.

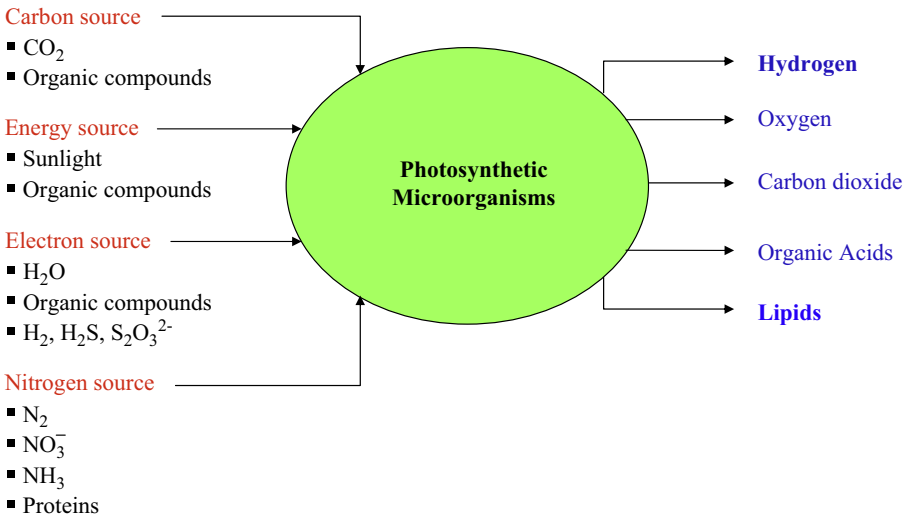

Fig. 3. Schematic of input and output of photosynthetic microorganisms consuming CO_2 and producing lipids or H_2.

human habitat or agriculture production [15]. In addition, CO_2 fixation using microalgae does not require CO_2 separation (concentration), and scrubbing of SO_x and NO_x prior to using the flue gas from fossil fuel power plants [20].

Moreover, microalgae produce other value-added by-products which can make the processes more economical. For example, some algal species are already used in medicinal and pharmaceutical products as well as health drinks for their immuno-stimulatory, antioxidant, anti-viral, and anticancer activities [21]. Others are incorporated in novel materials or used as fertilizer, in animal feed, in aquaculture, and stock material for biofuels [19,22]. Although photobiological fuel production by microorganisms presents various advantages over competing technologies, it is still in its infancy and faces numerous technical and economic challenges [23,24]. These challenges stem mainly from (i) inefficiencies in light utilization, (ii) large water and nutrient requirements during cultivation, and (iii) large auxiliary energy requirement during cultivation, harvesting and processing of the biomass and the biofuel [23–27] . All these challenges must be addressed for industrial-scale implementation of this technology. For further details, the reader is referred to recent literature reviewing the technical limitations, techno-economic and environmental analysis, as well as lifecycle analysis of this technology [23–27].

Photosynthetic microorganisms for fuel production are typically cultivated in systems known as photobioreactors (PBRs) which can have the form of open ponds (e.g., raceway ponds) or enclosures made of transparent tubes or panels [28]. Outdoor PBRs are the most inexpensive and have been used for decades. Unfortunately, current photobiological fuel production suffers from low solar to fuel conversion efficiency under outdoor conditions. For example, hydrogen production by microalgae is typically less than 1% efficient in outdoor PBRs [29]. Moreover, light transfer in photobioreactors is one of the main barriers to scaling the technology from bench top to industrial scale [30–32]. In addition, thermal management, water use, evaporation, and recycling, and contamination by other microorganisms that could compete for light and nutrients of PBRs content are also challenges encountered in large scale outdoor production.

Light utilization efficiency significantly affects the rest of the downstream processes and the overall biofuel production rate. Indeed, photosynthetic microorganisms require an optimum irradiance to achieve their maximum photosynthetic rate for the production of biofuels including biodiesel feedstock and H_2. In photobioreactors, they can suffer from:

- *Light inhibition*. Excessive irradiance inhibits the microbial photosynthesis and lipids or H_2 production through a process called photo-oxidative damage [19,33]. In outdoor systems, where this technology is meant to be deployed, solar irradiance can reach as high as 1000 W/m^2 [34]. For more efficient use of sunlight, it has to be redistributed uniformly throughout the PBR.
- *Limited light penetration*. Due to light absorption by both the microorganisms and the medium, and scattering by both the microorganisms and possibly gas bubbles, the local irradiance within the PBR may decrease below the required levels for photosynthesis, lipid production, and/or H_2 production [29,35–37]. This in turn limits the productivity and scale-up of the system.

Thus, careful radiation transfer analysis must be conducted to design and operate efficient PBRs for converting solar energy into biofuels by microorganisms. This paper discusses the importance of radiation transfer in the context of photobiological CO_2 fixation and biofuel production. It provides the reader with background information on light harvesting mechanisms by microorganisms, photosynthesis, and photobiological fuel production. It also reviews modeling efforts and experimental studies focusing on radiation transfer in PBRs.

2. Photobiological fuel production by microorganisms

A fuel is a substance that stores useful energy in its chemical bonds. Photosynthetic microbial cells can produce a large number of chemicals including sugars, lipids, and gases such as H_2 and CH_4. The chemicals can serve either as a fuel to directly power devices (e.g., fuel cells) or as a feedstock for producing other biofuels. In the production of these chemicals, solar energy serves as the primary energy source. The source of electrons incorporated in biofuels come (i) from reduced sulfur sources such as hydrogen sulfide (H_2S), sulfur (S^0), or thiosulfate ($S_2O_3^{2-}$) in photosynthetic bacteria and (ii) from water (H_2O) in plants, algae, and cyanobacteria [38].

2.1. Microbial electron generation and light harvesting pigments

Microbial electron generation begins with the absorption of photons by the photosynthetic apparatus. The latter consists of three major parts (i) the reaction center, (ii) the core antenna, and (iii) the peripheral antenna as illustrated in Fig. 4. Photochemical charge separation and electron transport take place in the reaction center [39]. The core antenna contains the minimum number of pigments necessary for photosynthesis and consisting only of chlorophylls or bacteriochlorophylls. It is surrounded by the peripheral antenna which is an assembly of chlorophylls, bacteriochlorophylls, and other accessory pigments such as carotenoids and phycobiliproteins. The peripheral antenna is particularly important in channeling additional photon energy to the reaction center at low light intensities. In algae and cyanobacteria, the photosynthetic apparatus is located on the photosynthetic membrane called thylakoid located inside the chloroplast as illustrated in the TEM micrograph of *Chlamydomonas reinhardtii* shown in Fig. 5 [40].

Different pigment molecules absorb at different spectral bands of the solar spectrum enabling more efficient utilization of solar energy. They also allow for the coexistence of different photosynthetic microorganisms by sharing different bands of the solar spectrum. Fig. 6 shows the absorption spectra of chlorophylls *a* and *b*, β-carotenoid, phycoerythrin, and phycocyanin over the spectral region from 400 to 700 nm, known as the photosynthetically active radiation (PAR) [39]. It also shows the profile of solar radiation spectrum (in arbitrary units) indicating that these pigments have evolved to absorb at

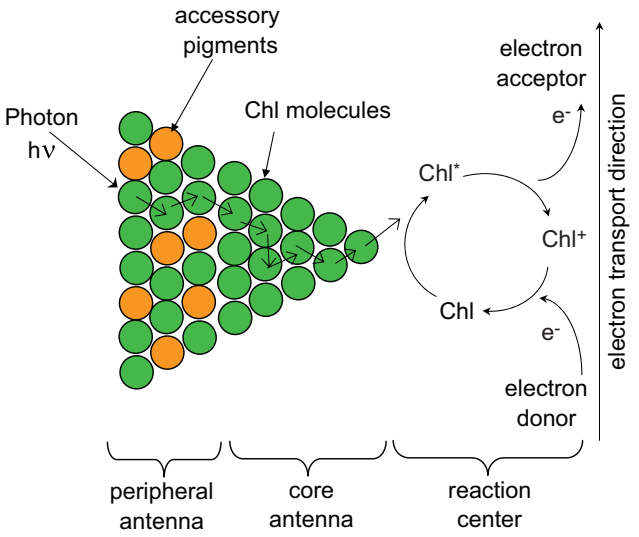

Fig. 4. Schematic of microbial electron generation and transport through the photosynthetic apparatus consisting of (i) the reaction center, (ii) the core antenna, and (iii) the peripheral antenna.

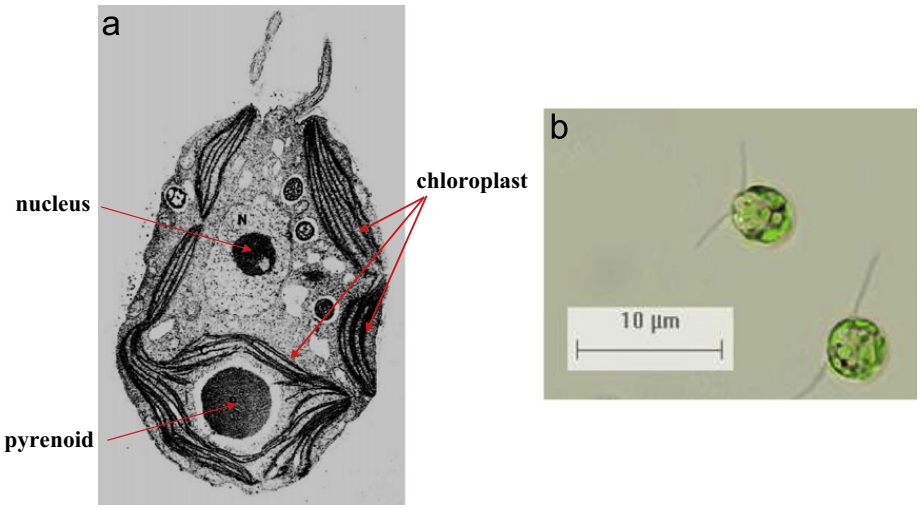

Fig. 5. (a) TEM micrograph of *Chlamydomonas reinhardtii* (Courtesy of Boynton) [40]. (b) Optical micrograph of *C. reinhardtii* showing typical ellipsoidal cell with major and minor diameters equal to about 9 and 8 μm, respectively [63].

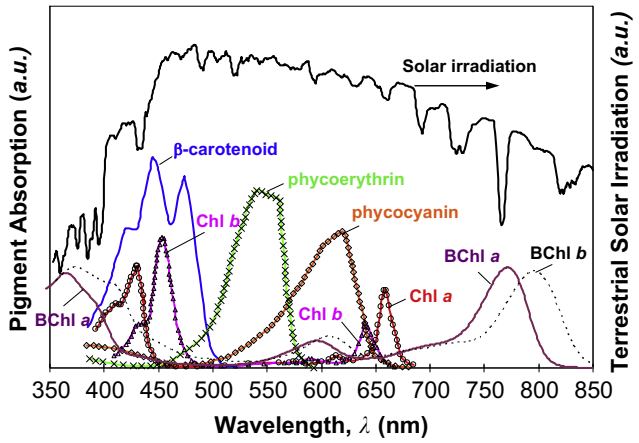

Fig. 6. Absorption spectra of β-carotenoid, phycoerythrin, phycocyanin, chlorophyll *a* (Chl *a*), chlorophyll *b* (Chl *b*), bacteriochlorophyll *a* (BChl *a*), and bacteriochlorophyll *b* (BChl *b*) in relation to the terrestrial solar irradiation spectrum (linear scale) [39]. The figure is in arbitrary units and the spectra of different molecules have been scaled arbitrarily for the sake of clarity.

wavelengths where the solar energy is most abundant. Each of the pigments used in the photosynthesis process is described in details in the next subsections.

2.1.1. Chlorophylls and bacteriochlorophylls

The main pigments necessary for oxygenic photosynthesis are called chlorophylls and those responsible for anoxygenic photosynthesis are called bacteriochlorophylls [38]. Fig. 6 shows that chlorophylls *a* and *b* have two absorption peaks, one in the blue and one in the red part of the visible spectrum [39]. Chlorophyll *a* absorbs around 430 and 680 nm while Chlorophyll *b* absorbs around 450 and 660 nm. Since they do not absorb green light ($\lambda \approx 520-570$ nm), they appear green to the human eye. These pigments are also responsible for the green color of plants. On the other hand, bacteriochlorophylls absorb light mainly in the far to near infrared part of the electromagnetic spectrum (700 nm $\leq \lambda \leq$ 1000 nm) [39].

2.1.2. Carotenoids

Carotenoids are accessory pigments found in all photosynthetic microorganisms. They absorb mainly in the blue part of the spectrum (400 nm $\leq \lambda \leq$ 550 nm) and are responsible for the yellow color of leafs in autumn and the orange color of carrots [39]. Carotenoids serve two major functions (i) shielding the photosynthetic apparatus from photo-oxidation under large light intensities and (ii) increasing the solar light utilization efficiency by expanding the absorption spectrum of the microorganism. They are hydrophobic pigments composed of long hydrocarbon chains and are embedded in the photosynthetic membrane. There are numerous carotenoids [39].

2.1.3. Phycobiliproteins

Phycobiliproteins are also accessory pigments that play a role in light harvesting and transferring this energy to the reaction centers. They are found in cyanobacteria and red algae [38]. Two major ones are phycoerythrin, absorbing mainly around 550 nm, and phycocyanin, absorbing strongly at 620 nm, as illustrated in Fig. 6 [38]. They are essential to the survival of these microorganisms at low light intensities.

2.2. Microbial photosynthesis and sugar production

Photosynthesis is a multi-step process by which plants, algae, and photosynthetic bacteria can store solar energy in the form of sugars using CO_2 as the carbon source. The overall reaction for photosynthesis is given by,

$$CO_2 + H_2O + light \rightarrow (CH_2O)_n + O_2 \quad (1)$$

Photosynthesis involves two types of reactions namely light and dark reactions. During light reactions, photons are absorbed by the microorganisms and are used to produce (i) adenosine triphosphate (ATP), the principal energy carrying molecule in cells and (ii) the electron carrier nicotinamide adenine dinucleotide phosphate (NADPH). These products of the light reaction are then used in the subsequent dark reactions including the Calvin cycle where CO_2 fixation takes place [39].

2.3. Microbial lipid production

Lipids produced by photosynthetic microorganisms include a broad group of molecules that are used in structural components of cells, energy storage, and cellular signaling [41]. The relevant group of lipids for fuel production is the triacylglycerols which are also known as neutral lipids [41,42]. Neutral lipid production is a complex, energy intensive multi-step process that takes place in the chloroplast of algae cells. Pathways for neutral lipid production can vary from species to species and are not fully understood [41]. However, on the most basic premise it has been proposed that neutral lipid production involves (i) first the synthesis of fatty acids using the products of photosynthesis as well as additional ATP and NADPH from light reactions as the energy and electron source, respectively, and (ii) reaction of these fatty acids in direct glycerol pathway to form triacylglycerols [43,44]. Both of these processes are significantly affected by physical factors such as total irradiance, spectral distribution of incident light, and temperature as well as the cell age and chemical factors such as nutrients, salinity and pH [45–55]. Among physical factors, irradiance has a major effect on altering the chemical composition of the produced lipids [50–55]. Although the effects vary among different species, in most photosynthetic microorganisms, low irradiance results in the synthesis of fatty acids mostly used in structural polar lipid production whereas high irradiance increases the neutral lipid production and accumulation in cells under light saturated conditions [54,55].

2.4. Microbial hydrogen production

Photobiological processes resulting in hydrogen production in microbes can be grouped into three categories namely: (1) direct biophotolysis using green algae, (2) indirect biophotolysis using cyanobacteria, and (3) photofermentation using photosynthetic bacteria [56].

2.4.1. Direct biophotolysis

In this mechanism H_2 is produced by diverting the electrons generated from water splitting from the Calvin cycle to the bidirectional hydrogenase enzyme [57]. This mechanism is theoretically the most energy efficient mechanism of H_2 production with a theoretical maximum of 40.1% [58]. Green algae such as *C. reinhardtii*, *Chlamydomonas moewusii*, *Scenedesmus obliquus*, and *Chlorococcum littorale* are capable of producing H_2 via direct biophotolysis [57]. However O_2 gas is also produced during this process and may irreversibly inhibit the functioning of the hydrogenase enzyme.

2.4.2. Indirect biophotolysis

The source of electrons in indirect biophotolysis is also water. However, in this mechanism, the electrons are first used to reduce CO_2 into organic compounds during photosynthesis. Then, the electrons are derived from the degradation of the organic compounds and used in generating H_2 through the action of nitrogenase [59]. Due to the facts that: (i) multiple steps are involved in converting solar energy to H_2 and (ii) the use of nitrogenase enzyme requires ATP, the maximum possible light to H_2 energy conversion efficiency of indirect biophotolysis is only 16.3% [58]. Cyanobacteria such as *Anabaena variabilis*, *Anabaena azollae*, *Nostoc muscorum* IAM M-14, and *Oscillatoria limosa* are capable of indirect biophotolysis [60]. In this process, a nearly pure stream of H_2 is produced, unlike in direct biophotolysis.

2.4.3. Photo-fermentation

In this mechanism, extracellular organic materials (e.g. organic acids, carbohydrates, starch, and cellulose [61]) are used as the electron source and solar energy is used as an energy source to produce H_2 by nitrogenase enzyme [57]. This mechanism is viewed as the most promising microbial system to produce H_2 [57]. Purple non-sulfur bacteria such as *Rhodobacter sphaeroides*, *Rhodospirillum rubum*, and *Rhodopseudomonas sphaeroides* are examples of photo-fermentative H_2 producers.

3. Modeling radiation transfer in photobioreactors

As light penetrates in the photobioreactor, it is absorbed by the microorganisms or by the medium and scattered by microorganisms and, possibly, by gas bubbles used to deliver CO_2 and to stir the suspension. Microorganisms are $1-10\,\mu m$ in diameter and are much larger than the wavelengths in the PAR. Therefore, the size parameter is larger than 4 and scattering is strongly forward [62,63]. In addition, the refractive index relative to that of water ranges from 1.04 to 1.07 and changes by ± 0.01 over the spectral range from 350 to 750 nm. The absorption index is about 0.003 and varies by ± 0.003 over the same spectral range [65]. On the other hand, the refractive index of the medium is typically assumed to be that of water reported by Hale and Querry [64]. This section describes the simulation and modeling tools developed to design, scale-up, optimize, and compare the various photobioreactor designs. These tools relate local spectral light intensity I_λ (in $W/m^2\,\mu m\,sr$) or spectral fluence rate G_λ (in $W/m^2\,\mu m$) with microorganism growth and lipid or H_2 production. The reader is referred to Refs. [65–67] for a review of the different photobioreactor designs, operation, and associated challenges.

3.1. Radiation transfer through microorganisms suspensions

Solar radiation intensity $I_\lambda(z,\hat{s})$ (in $W/m^2\,\mu m\,sr$) at a given location $\hat{r}$ in the direction $\hat{s}$ in photobioreactors or open ponds containing an absorbing, scattering, and non-emitting microorganisms in suspensions along with bubbles is composed of a collimated and a diffuse component, denoted by $I_{c,\lambda}(\hat{r},\hat{s})$ and $I_{d,\lambda}(\hat{r},\hat{s})$, respectively, and can be written as [68],

$$I_\lambda(\hat{r},\hat{s}) = I_{c,\lambda}(\hat{r},\hat{s}) + I_{d,\lambda}(\hat{r},\hat{s}) \tag{2}$$

The intensity I_λ can be determined by solving the radiative transfer equation (RTE) which is an energy balance on the radiative energy traveling along a particular direction $\hat{s}$. The steady-state RTE for the collimated intensity can be

written as [68]

$$\hat{s}\cdot\nabla I_{c,\lambda}(\hat{r},\hat{s}) = -\beta_{eff,\lambda} I_{c,\lambda}(\hat{r},\hat{s}) \tag{3}$$

where $\beta_{eff,\lambda}$ is the effective extinction coefficient expressed as

$$\beta_{eff,\lambda} = \kappa_{eff,\lambda} + \sigma_{eff,\lambda} \tag{4}$$

Here, $\kappa_{eff,\lambda}$ and $\sigma_{eff,\lambda}$ are the effective absorption and scattering coefficients (in m^{-1}) of the photobioreactor content.

Moreover, the steady-state RTE for the diffuse intensity $I_{d,\lambda}(\hat{r},\hat{s})$ can be written as [68]

$$\begin{aligned}\hat{s}\cdot\nabla I_{d,\lambda} = &-\kappa_{eff,\lambda} I_{d,\lambda}(\hat{r},\hat{s}) - \sigma_{eff,\lambda} I_{d,\lambda}(\hat{r},\hat{s})\\ &+\frac{\sigma_{eff,\lambda}}{4\pi}\int_{4\pi} I_{d,\lambda}(\hat{r},\hat{s}_i)\Phi_{eff,\lambda}(\hat{s}_i,\hat{s})\,\mathrm{d}\Omega_i\\ &+\frac{\sigma_{eff,\lambda}}{4\pi}\int_{4\pi} I_{c,\lambda}(\hat{r},\hat{s}_i)\Phi_{eff,\lambda}(\hat{s}_i,\hat{s})\,\mathrm{d}\Omega_i\end{aligned} \tag{5}$$

where $\Phi_{eff,\lambda}(\hat{s}_i,\hat{s})$ is the effective scattering phase function. It represents the probability that radiation traveling in the solid angle $\mathrm{d}\Omega_i$ around the direction $\hat{s}_i$ will be scattered into the solid angle $\mathrm{d}\Omega$ around the direction $\hat{s}$. The first integral term in Eq. (5) accounts for the in-scattered diffuse radiation whereas the second term corresponds to the in-scattered collimated radiation.

The effective absorption coefficient $\kappa_{eff,\lambda}$ accounts for the absorption by the liquid phase and by the microorganisms at wavelength λ. It can be written in terms of the bubble volume fraction f_B and of the microorganism concentration N expressed in number of cells per m^3 of suspension

$$\kappa_{eff,\lambda} = \kappa_{L,\lambda}(1-f_B-N v_N) + A_{abs,\lambda} N \tag{6}$$

where v_N is the volume occupied by a single microorganism. The term Nv_N represents the total volume fraction of photobioreactor occupied by microorganisms. The absorption coefficient of the liquid phase $\kappa_{L,\lambda}$ is expressed in m^{-1}, and the mass absorption cross-section of a microorganism $A_{abs,\lambda}$ is expressed in m^2. The product $\kappa_{N,\lambda} = A_{abs,\lambda} N$ corresponds the absorption coefficient (in m^{-1}) of the microorganism suspension without bubble. Note that the microorganisms concentration X (expressed in kg dry cell weight per m^3 of liquid medium, or simply in kg/m^3) can also be used; then A_{abs} and S_{sca} are expressed in m^2/kg [62].

Similarly, assuming independent scattering and monodisperse bubbles of radius a, the effective scattering coefficient of the composite medium $\sigma_{eff,\lambda}$ can be expressed as the sum of the scattering coefficients of the microorganisms $\sigma_{N,\lambda}$ and of the bubbles $\sigma_{B,\lambda}$ as [69],

$$\sigma_{eff,\lambda} = \sigma_{N,\lambda} + \sigma_{B,\lambda} = S_{sca,\lambda} N + \frac{A_i}{4} Q_{sca,B}(a,\lambda) \tag{7}$$

where $S_{sca,\lambda}$ is the mass scattering cross-section of a microorganism expressed in m^2 and $Q_{sca,B}(a,\lambda)$ is the scattering efficiency factor of a bubble of radius a at wavelength λ obtained from Mie theory [70]. The interfacial area concentration A_i is defined as the total surface area of monodisperse bubbles per unit volume and expressed as $A_i = 3f_B/a$. A similar approach can be used to model (i) mixed cultures, (ii) scattering by beads in packed bed photobioreactors, and/or (iii) polydisperse bubbles [68], for example. Note that, in the ocean optics literature, the variables κ_λ, σ_λ, β_λ, and Φ_λ are often denoted by a_λ, b_λ, c_λ, and β_λ, respectively [71–73]. Here, the nomenclature commonly used in the radiative heat transfer community is employed [68].

The effective scattering phase function of the suspension containing microorganisms and bubbles $\Phi_{eff,\lambda}$ can be defined as [74]

$$\Phi_{eff,\lambda}(\hat{s}_i,\hat{s}) = \frac{\sigma_{N,\lambda}\Phi_{N,\lambda}(\hat{s}_i,\hat{s}) + \sigma_{B,\lambda}\Phi_{B,\lambda}(\hat{s}_i,\hat{s})}{\sigma_{N,\lambda}+\sigma_{B,\lambda}} \tag{8}$$

where $\Phi_{N,\lambda}(\hat{s}_i,\hat{s})$ and $\Phi_{B,\lambda}(\hat{s}_i,\hat{s})$ are the scattering phase functions of the microorganisms and the bubbles, respectively. The effective scattering phase function is normalized such that,

$$\frac{1}{4\pi}\int_{4\pi}\Phi_{eff,\lambda}(\hat{s}_i,\hat{s})\,\mathrm{d}\Omega_i = 1 \tag{9}$$

The Henyey–Greenstein phase function is often used as an approximate phase function for its simplicity and its ability to capture a wide range a scattering behavior from strongly backward to strongly forward. It is given by [68]

$$\Phi_{HG,\lambda}(\Theta) = \frac{1-g_\lambda^2}{[1+g_\lambda^2-2g_\lambda\cos\Theta]^{3/2}} \tag{10}$$

where Θ is the scattering angle between $\hat{s}_i$ and $\hat{s}$ while g_λ is the so-called Henyey–Greenstein asymmetry factor defined as the mean cosine of the scattering phase function defined as [68]

$$g_\lambda = \frac{1}{4\pi}\int_{4\pi}\Phi_\lambda(\Theta)\cos\Theta\,\mathrm{d}\Omega \tag{11}$$

For strongly forward scattering observed in microalgal suspensions, g_λ approaches unity while it is equal to zero for isotropic scattering.

Finally, the RTE given by Equations (3) and (5) indicates that the absorption and scattering coefficients of microalgae together with the scattering phase function are major parameters needed to solve the radiation transfer equation and predict light transfer in photobioreactors or ponds for simulation, design and optimization purposes. However, these characteristics are strongly dependent on wavelength and difficult to predict from electromagnetic wave theory given the complex morphology of the microorganisms and their various chromophores [75]. Instead, they can be directly measured experimentally as discussed in Section 4.

3.2. Solutions of the RTE in photobioreactors

3.2.1. Beer-Lambert's law

Beer-Lambert's law provides the solution of the one-dimensional steady-state RTE accounting for both absorption and out-scattering but ignoring in-scattering. It physically corresponds to cases when photons experience at most one scattering event as they travel through the reactor, i.e., single scattering prevails. It gives the local spectral fluence rate $G_\lambda(z)$ within the photobioreactor

defined as

$$G_\lambda(z) = \int_0^{4\pi} I_\lambda(z,\hat{s})\, \mathrm{d}\Omega = G_{\lambda,in}\, \exp(-\beta_{eff,\lambda} z) \tag{12}$$

where $G_{\lambda,in}$ is the spectral irradiance incident on the photobioreactor, z is the distance from the front surface. Beer-Lambert's law has been used extensively to predict the local fluence rate within photobioreactors [76,77]. However, this method ignores in-scattering and can lead to unacceptable errors in predicting fluence rate profile in photobioreactors of thickness L containing an optically thick suspension such that $\beta_{eff,\lambda} L \gg 1$ and multiple scattering prevails.

3.2.2. Two-flux approximation

Cornet et al. [35–37] solved the radiative transfer equation (RTE) using the Schuster–Schwarzschild two-flux approximation to model light transfer in filamentous cyanobacterium *Spirulina platensis* cultures. This approach consists of solving two coupled ordinary differential equations obtained by integrating the one-dimensional RTE over two complementary hemispheres. It can account for in-scattering terms as well as anisotropic scattering [68]. It can also provide an analytical solution for $G_\lambda(z)$, albeit more complex than Beer-Lambert's law [75,78,79]. For example, Pottier et al. [75] derived an expression for the local fluence rate $G_\lambda(z)$ (in W/m^2) in a one-dimensional flat plate photobioreactor, with a transparent front window and a diffusely reflecting back side of reflectance ρ, exposed to solar irradiance $G_{in,\lambda}$ incident onto the photobioreactor with an angle θ_c with respect to the normal direction as

$$\frac{G_\lambda(z)}{G_{in,\lambda}} = 2\sec\theta_c \times \frac{[\rho_\lambda(1+\alpha_\lambda)e^{-\delta_\lambda L} - (1-\alpha_\lambda)e^{-\delta_\lambda L}]e^{\delta_\lambda z} + [(1+\alpha_\lambda)e^{\delta_\lambda L} - \rho_\lambda(1-\alpha_\lambda)e^{\delta_\lambda L}]e^{-\delta_\lambda z}}{(1+\alpha_\lambda)^2 e^{\delta_\lambda L} - (1-\alpha_\lambda)^2 e^{-\delta_\lambda L} - \rho_\lambda(1-\alpha_\lambda^2)e^{\delta_\lambda L} + \rho_\lambda(1-\alpha_\lambda^2)e^{-\delta_\lambda L}} \tag{13}$$

where α_λ and δ_λ are expressed as [75]

$$\alpha_\lambda = \sqrt{\frac{A_{abs,\lambda}}{A_{abs,\lambda} + 2b_\lambda S_{sca,\lambda}}} \quad \text{and}$$

$$\delta_\lambda = N \sec\theta_c \sqrt{A_{abs,\lambda}(A_{abs,\lambda} + 2b_\lambda S_{sca,\lambda})} \tag{14}$$

Here, b_λ is the backward scattering fraction defined as

$$b_\lambda = \frac{1}{2}\int_{\pi/2}^{\pi} \Phi_\lambda(\theta)\sin\theta\, \mathrm{d}\theta \tag{15}$$

Note that for outdoor photobioreactors, the incident irradiance on the reactor surface can be expressed as $G_{in} = G_{\lambda,s}\cos\theta_c$ where $G_{\lambda,s}$ is the direct solar hemispherical irradiance shown in Fig. 1. Pottier et al. [75] experimentally validated the above expression for the local fluence rate $G_\lambda(z)$ by measuring in-situ the local irradiance in a torus photobioreactor containing a suspension of *C. reinhardtii* using a spherical quantum sensors.

3.2.3. Discrete ordinate methods

Most of the above-mentioned studies did not account for the spectral dependency of the radiation characteristics and/or for the presence of bubbles often used in actual photobioreactors. More recently, Berberoğlu et al. [69] simulated light transfer in a bubble sparged photobioreactor accounting for absorption and anisotropic scattering by both bubbles and filamentous cyanobacterium *A. variabilis*. One-dimensional light transfer modeling was performed by solving the RTE using the discrete ordinate method (DOM) on a spectral basis. Spectral variations of radiation characteristics over the spectral range from 400 to 700 nm were accounted for using the box model [69]. Genetically engineered microorganisms with reduced pigment content were also considered. The authors established that: (i) Beer-Lambert's law cannot be applied to predict the fluence rate inside the photobioreactor, i.e., multiple scattering must be accounted for, (ii) isotropic scattering can be assumed for wild strain microorganisms for all practical purposes in the absence of bubbles in the photobioreactor, (iii) anisotropic scattering by the bubbles must be taken into account for all microorganism concentrations and particularly as the interfacial area concentration increases due to large gas volume fraction and/or smaller bubble radius, (iv) for microorganisms with reduced pigment concentrations, anisotropic scattering dominates over absorption (see Section 5.1) and should be considered in computing the local fluence rate.

Fig. 7 shows the local fluence rate in a planar photobioreactor with a transparent front window and a black back wall ($\rho = 0$) containing filamentous microorganisms with concentration X and monodisperse spherical bubbles with interfacial area concentration A_i. The fluence rate was predicted by: (i) Beer-Lambert's law and using DOM method assuming (ii) isotropic scattering ($g_\lambda = 0.0$), and (iii) approximate anisotropic scattering based on the Henyey-Greenstein asymmetry factor g_λ predicted from the Mie theory. Four different cases were considered with low and high microorganism concentrations X equal to 0.035 and 0.35 kg/m^3 and bubble interfacial area concentration A_i equal to 0 and 1500 m^2/m^3 corresponding to different values of effective single scattering albedo defined as $\omega_{eff} = \sigma_{eff}/\beta_{eff}$.

3.3. Coupling light transfer to microbial kinetics

3.3.1. Growth kinetics

During the growth phase, the time rate of change of microorganism cell density N can be modeled as [80]

$$\frac{\mathrm{d}N}{\mathrm{d}t} = \mu N \tag{16}$$

where μ is the specific growth rate expressed in s^{-1} and function of the average available fluence rate denoted by G_{av}. The specific growth rate has been modeled using the Monod model taking into account light saturation and inhibition as [65]

$$\mu = \mu_{max}\left(\frac{G_{av}}{K_{s,G} + G_{av} + G_{av}^2/K_{i,G}}\right) \tag{17}$$

where μ_{max} is the maximum specific growth rate while the coefficients $K_{s,G}$ and $K_{i,G}$ are the light half-saturation and inhibition constants, respectively. Similar models can be formulated to account for saturation and inhibition

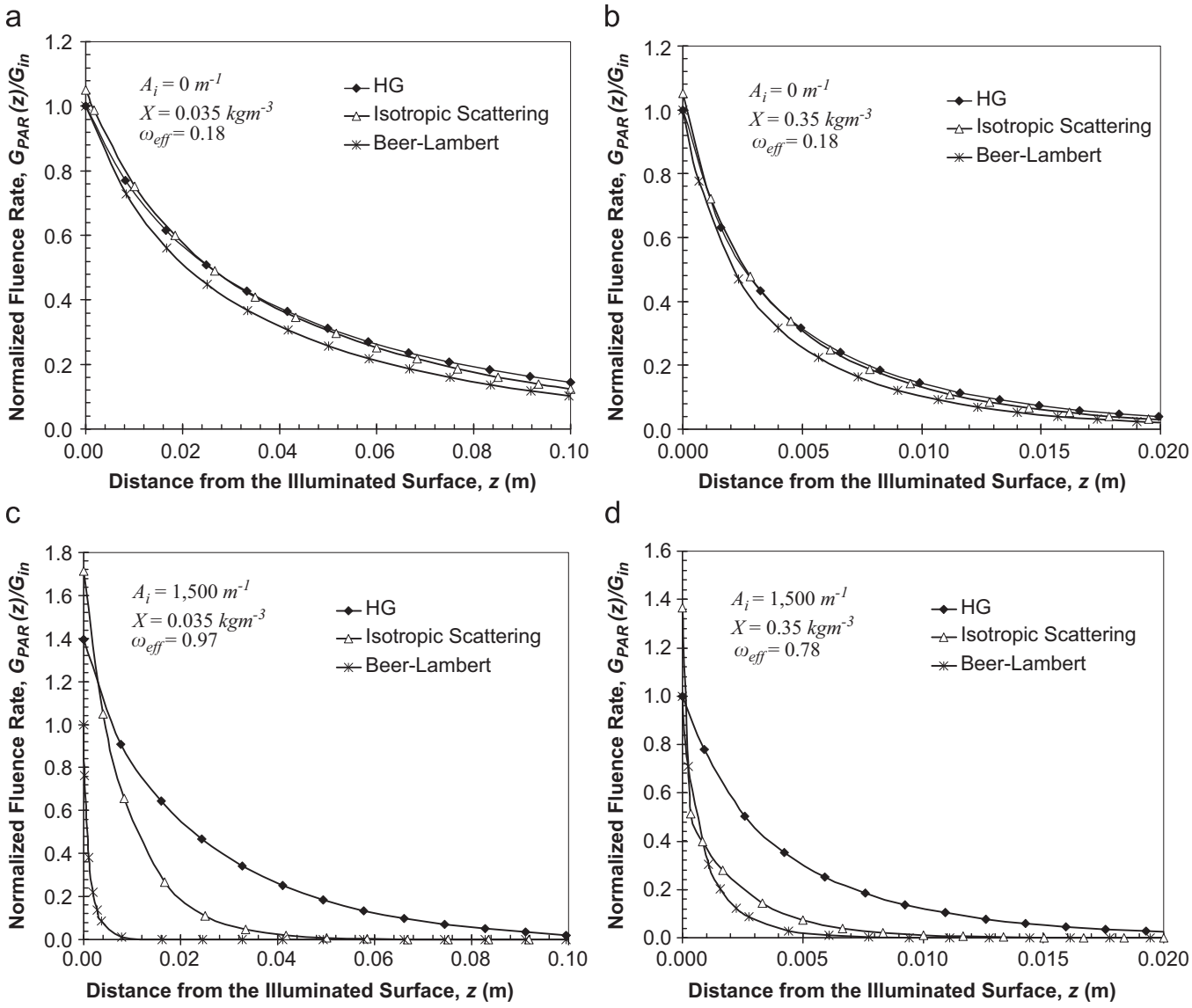

Fig. 7. Normalized local fluence rate over the PAR as a function of the distance from the illuminated surface for different phase functions (isotropic, Henyey-Greenstein (HG)) and values of bubble interfacial area concentrations A_i and microorganism concentrations X (a) A_i=0 m^{-1} and X=0.035 kg dry cell/m^3, (b) A_i=0 m^{-1} and X=0.35 kg dry cell/m^3, (c) A_i=1,500 m^{-1} and X=0.035 kg dry cell/m^3 and (d) A_i=1500 m^{-1} and X=0.35 kg dry cell/m^3 (after Berberğlu et al. [69]).

due to limited or excessive carbon dioxide concentrations or excessive microorganism concentrations, for example. The average available fluence rate G_{av} can be estimated by averaging the local fluence rate over the depth of the culture L as

$$G_{av} = \frac{1}{L}\int_0^L G_{PAR}(z)\,dz = \frac{1}{L}\int_0^L \left(\int_{PAR} G_\lambda(z)\,d\lambda\right)dz \qquad (18)$$

where $G_\lambda(z)$ is estimated by: (i) solving the RTE, (ii) using approximate solutions such as Beer-Lambert's law [Eq. (12)] or two flux approximation [Eq. (13)], or (iii) averaging the light energy received by microorganisms as predicted by hydrodynamics simulations. Integration over wavelength is performed over the PAR between 400 and 700 nm to give the local PAR-averaged fluence rate denoted by $G_{PAR}(z)$.

Typical variation of growth rate with respect to incident light intensity has three distinct regions as illustrated in Fig. 8. Region 1 features increasing growth rate with increasing fluence rate as light limitation is overcome. By contrast, in region 2, the growth rate is constant and independent of light. Finally, region 3 corresponds to light inhibition when the growth rate decreases as fluence rate increases. These three regions depend strongly on the species and external factors such as temperature, CO_2 concentration, and nutrients. It is important to note that from the perspective of light to biomass energy efficiency, operating at the intersection of regions 1 and 2 is optimal.

Moreover, photosynthetic organisms were experimentally found to be more prone to light inhibition at lower temperatures [81,82]. For example, Sorokin and Krauss [82] found that the saturation fluence rate $K_{s,G}$ for *Chlorella pyrenoidosa* was 5328 lux at 25 °C while it was 15,069 lux at 39 °C. Similarly, the authors showed that the fluence rate in Region 3 at which the growth rate

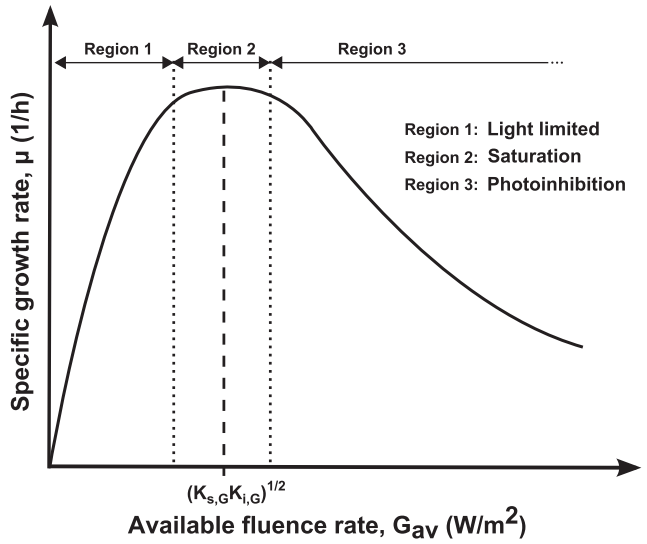

Fig. 8. Typical specific growth rate μ as a function of average available fluence rate in the PAR given by Eq. (17).

declined to half of its maximum value was 37,674 and 91,493 lux for the same temperatures. They also tested several other species of algae and found these to be typical values. Note that direct sunlight can reach intensities up to 110,000 lux [9,68].

3.3.2. Photobiological fuel evolution kinetics

The specific biofuel production rate π can been modeled with a Michaelis–Menten type equation given by [80]

$$\pi = \pi_{max} \frac{G_{av}}{K_{s,prod} + G_{av} + G_{av}^2/K_{i,prod}} \tag{19}$$

where π_{max} is the maximum specific production rate expressed in kg of product/kg dry cell/h. The parameters $K_{s,prod}$ and $K_{i,prod}$ account for the saturation and the inhibition of fuel production due to excessive irradiation or limited light fluence rate, respectively. However, due to the complexity of biofuel production and its high sensitivity to physical and chemical factors and to the cell age, the success of obtaining a consistent set of model parameters for Eq. (19) has been challenging. Berberoğlu and Pilon [83] used this methodology to model the hydrogen production of green algae and purple non-sulfur bacteria based on the experimental data reported by Nogi et al. [84].

3.4. Performance assessment

3.4.1. Incident light

Incident light irradiance G_{in} is often reported (1) in total luminous flux expressed in lux (1 lux=1 cd sr/m^2), (2) in photon flux expressed in μmol/m^2/s, or (3) in energy flux expressed in W/m^2. The total luminous flux, also known as illuminance, is a photometric unit which measures light accounting for the human eye sensitivity. The energy emitted by the source is wavelength weighted by the luminosity function, which describes the average sensitivity of the human eye to light at different wavelengths between 400 and 700 nm. Different light sources with different emission spectra could have the same illuminance. On the other hand, photon flux refers to the number of moles of photons (6.02×10^{23} photons per mole) incident on a unit surface area per unit time. In studies of photosynthetic systems, the photon flux is typically measured over the PAR with a calibrated quantum sensor. However, both illuminance and the PAR-photon flux apply only in the spectral range from 400 to 700 nm and cannot be used to quantify energy in the near infrared (NIR) part of the spectrum. Thus, in experiments using microorganisms that absorb in NIR, such as purple non-sulfur bacteria [62], illumination reported in illuminance or photon flux cannot be used. Ideally, the spectral radiation flux should be reported in W/m^2 μm and recorded with a pyranometer having sensitivity from about 300 to 2800 nm. Moreover, for bench top experiments using artificial light, it is recommended that the emission spectrum of the light source be also reported for clarity and reproducibility of the experiments. It is useful to report not only the total but also the spectral incident irradiance. This enables unit conversion and comparison with other studies.

3.4.2. Light to biomass energy conversion efficiency

The instantaneous light to biomass energy conversion efficiency is defined as [85]

$$\eta_b = \frac{(V_L \sigma_b \gamma_b Q_o)/M_C}{G_{in} A_s} \frac{\mathrm{d}X}{\mathrm{d}t} \tag{20}$$

where $\mathrm{d}X/\mathrm{d}t$ is the time rate of change of the microorganism concentration, expressed in kg dry cell/m^3/s. The volume of the microorganism suspension in the photobioreactor is denoted by V_L and initially equals V_o. Furthermore, Q_o is the energy content of biomass per available electron (in J/#e) and M_C is the molar mass of carbon equal to 0.012 kg/mol. Moreover, σ_b is the mass fraction of carbon in the biomass and γ_b is the degree of reductance of the biomass, i.e., the number of available electrons per mol of carbon in the biomass, expressed in #e/mol. The values of σ_b and γ_b depend on the elemental composition of the biomass given as $CH_pO_nN_q$, where p, n, and q are the average numbers of hydrogen, oxygen, and nitrogen atoms per carbon atom in the biomass. In addition, the degree of reductance is defined as $\gamma_b = 4+p-2n-3q$ (in #e/mol). Finally, G_{in} is the total irradiance incident on the photobioreactor of surface area A_s.

The photosystems I and II each require 4 moles of photons of wavelength equal to or smaller than 700 and 680 nm (red), respectively, to fix 1 mole of CO_2 [13]. The thermodynamic efficiency of photosynthesis is defined as the energy required to produce 1 mole of simple sugar (hexose, $C_6H_{12}O_6$) divided by the amount of energy from the incident light (177 kJ/mol of photons at 680–700 nm) [39]. In an idealized system where the photon requirements of the photosystems is spectrally matched with a light source only emitting these characteristic wavelengths, the thermodynamic limit of photosynthesis is about 34% [13,39]. However, based on the global AM 1.5 terrestrial solar energy spectrum, the theoretical limit of terrestrial photosynthesis is estimated to be

13% [13]. Note also that exposing plants and algae to only red light is sufficient to carry out photosynthesis and results in the same growth rates as with white light [86–88]. This is due to red light absorption by photosystem II where light reactions (the first stage of photosynthesis) start.

3.4.3. Light to biofuel energy conversion efficiency

Similarly, light to biofuel energy conversion efficiency of photobioreactors is defined as the ratio of the energy that would be released from the combustion of the produced biofuel to the energy input to the system as light and can be expressed as [90]

$$\eta_{prod} = \frac{\Delta\Gamma R_{prod}}{G_{in} A_s} \tag{21}$$

where R_{prod} is the rate of biofuel production in mol/s and $\Delta\Gamma$ is the Gibbs free energy of the produced fuel in J/mol at 25 °C and 101.325 kPa. For hydrogen production, $\Delta\Gamma = \Delta\Gamma_o - RT\ln(P_o/P_{H_2})$ where $\Delta\Gamma_o$ is the standard-state free energy of formation of H_2 from the water splitting reaction, equal to 236,337 J/mol at 303 K. The term $RT\ln(P_o/P_{H_2})$ is the correction factor for $\Delta\Gamma_o$ when H_2 production takes place at H_2 partial pressure P_{H_2} instead of the standard pressure P_o of 1 atm. Note that in reporting the light energy conversion efficiency, it is important to report the spectral range over which G_{in} is measured. Indeed, the efficiency computed using G_{in} defined over the PAR is about 2.22 times larger than that obtained with G_{in} computed over the entire solar spectrum.

4. Experimental measurements of radiation characteristics of microalgae

In order to simulate light transfer in photobioreactors and use any of the above-mentioned light transfer models, the spectral radiative characteristics, namely, $\kappa_{N,\lambda}$, $\sigma_{N,\lambda}$, and $\Phi_{N,\lambda}(\hat{s}_i,\hat{s})$ of the microorganisms are required. They can be determined either through experimental measurements [62,63] or theoretically by using Mie theory [75]. Theoretical predictions often assume that the scatterers have relatively simple shape (e.g., spherical) and ignore their heterogeneous nature by assuming that the complex index of refraction is uniform. Pottier et al. [75] acknowledged that for complex microorganisms shapes (e.g., cylinders and spheroids), advanced numerical tools are required to predict radiative characteristics. Alternatively, experimental measurements account for the actual shape and morphology and size distribution of the microorganisms. A comprehensive review of the experimental techniques for measuring the radiation characteristics has been reported by Agrawal and Mengüç [91] and need not be repeated. The following sections summarize experimental techniques specifically used to measure the radiation characteristics of microorganisms.

4.1. Typical assumptions

In measuring the radiation characteristics, the following assumptions are typically made: (1) the microorganisms are well mixed (i.e., randomly distributed) and randomly oriented, (2) for all measurements, the pathlength and concentration of the samples are such that single scattering prevails, i.e., photons undergo one scattering event at most as they travel through the suspension, (3) the scattering phase function has azimuthal symmetry and is only a function of the polar angle [68]. The single scattering regime prevails if the sample thickness t is much smaller than the photon mean free path l_p such that [92,93],

$$t(1-g_{N,\lambda}) \ll l_{p,\lambda} \tag{22}$$

where $l_{p,\lambda} = 1/\beta_{N,\lambda}$ and $g_{N,\lambda}$ is the Henyey–Greenstein asymmetry factor.

4.2. Scattering phase function, $\Phi_{N,\lambda}(\hat{s}_i,\hat{s})$

The scattering phase function $\Phi_{N,\lambda}(\hat{s}_i,\hat{s})$ of microorganisms can be measured using a nephelometer [94]. A typical nephelometer comprises a detector with a small acceptance angle that can measure the scattered radiation as a function of the polar and the azimuthal angles. A recent review of different nephelometer designs was given by Jonasz and Fournier [93]. For spherical or randomly oriented particles, as in the case of well mixed microorganism suspensions, the phase function does not change as a function of the azimuthal angle [68]. Thus, most nephelometers measure $\Phi_{N,\lambda}$ as a function of the polar angle Θ only. Moreover, the scattering phase function for large particles does not vary significantly with wavelength at scattering angles less than 15° [71]. Since most of the scattered light is in the forward direction, phase function measurements taken at 632.8 nm can be used as a first order approximation for modeling light transfer in photobioreactors over the PAR.

Fig. 9 shows the schematic of the experimental setup assembled by Berberoğlu and Pilon [62,63] and inspired from that assembled by Incropera and co-workers [95,96]. In brief, a He–Ne laser provided a continuous monochromatic laser beam at 632.8 nm. It was modulated by a beam chopper and collimated with a set of collimating lenses and a pinhole. The collimated beam entered a custom-made sample holder dish containing the microorganism suspension through a transparent glass window as shown in Fig. 9a. The dish was made of aluminum and painted with Krylon ultra flat black spray paint. The sides of the dish were banked at 45° to minimize reflections within the container. The microalgae were kept in suspension with the aid of a black magnetic stirring bar and a magnetic stirrer. The scattered light was collected with a custom-made fiber-optic probe consisting of (i) a miniaturized Gershun tube with a small acceptance angle and (ii) a solarization resistant UV-IR fiber-optic cable. Fig. 9c shows the geometry and the dimensions of the Gershun tube. The probe was mounted on a computer-controlled motorized rotary stage. Due to finite beam diameter, the fiber-optic probe blocks the incident beam at scattering angles greater than 160°. Therefore, data could only be obtained for scattering angles up to 160°. The scattered light intensity at scattering angle Θ denoted by $I_\lambda(\Theta)$ was measured by a photomultiplier tube (PMT) and amplified with a lock-in amplifier. The PMT was powered with a

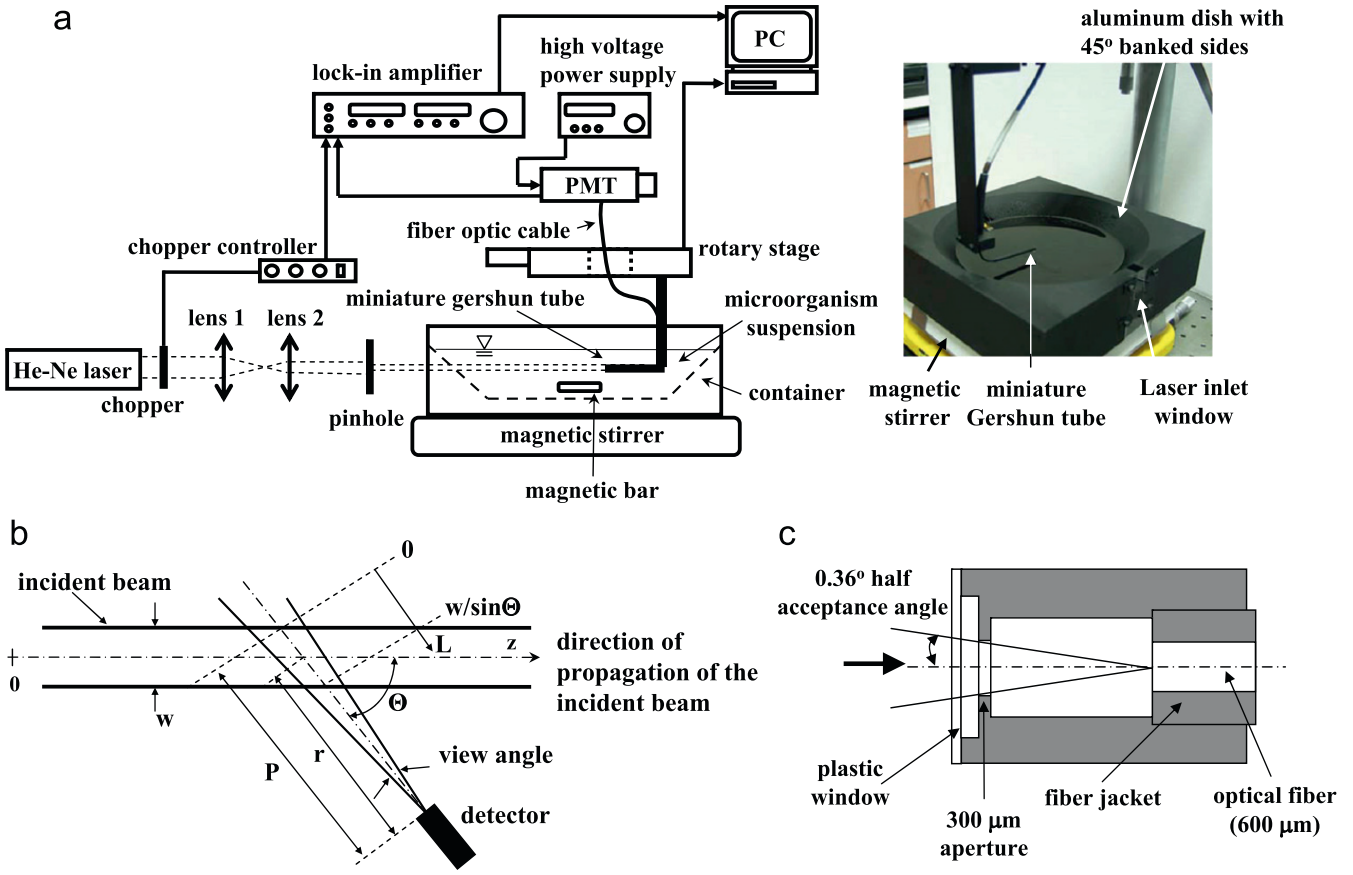

Fig. 9. Schematic of (a) the nephelometer used to measure the scattering phase function at 632.8 nm, (b) the miniaturized Gershun tube (drawings not to scale). Coordinate system used in recovering the scattering phase function from the measured intensity distribution [123].

variable high voltage power supply. The latter enables the sensitivity of the PMT to be varied so that the input to the lock-in amplifier was within its detection range. Synchronization of the lock-in amplifier together with the beam chopper enables the detection of noisy signals otherwise difficult to detect.

The scattering phase function can be recovered using the analysis suggested by Daniel and Incropera [95,96],

$$\Phi_{N,\lambda}(\Theta) = \frac{2I_\lambda(\Theta)[U_\lambda(\Theta)]^{-1}}{\int_0^\pi I_\lambda(\Theta)[U_\lambda(\Theta)]^{-1}\sin\Theta\,\mathrm{d}\Theta} \tag{23}$$

The term $U_\lambda(\Theta)$ is a geometrical correction term defined as [95,96]

$$U_\lambda(\Theta) = \int_0^{w/\sin\Theta}\left[1+\beta_{N,\lambda}\frac{w}{2}\cot\Theta-\beta_{N,\lambda}L\cos\Theta\right]\times\left[1-\beta_{N,\lambda}\left(r-\frac{w}{2\sin\Theta}\right)\right]\times\left[1-\beta_{N,\lambda}\left(\frac{w}{\sin\Theta}-L\right)\right]\mathrm{d}L \tag{24}$$

where w is the beam diameter in m, r is the radius of rotation of the fiber-optic probe and L is the coordinate direction along the line of sight of the detector, marking the length of the scattering volume as shown in Fig. 9b. The pathlength of the radiation reaching the detector is denoted by $P = w/2\sin\Theta + r$ [96]. At all angles, the value of $\beta_{N,\lambda}P$ should be less than 0.1 to ensure single scattering [96].

4.3. Absorption coefficient, $\kappa_{N,\lambda}$

A large body of literature exists on measuring the absorption coefficient $\kappa_{N,\lambda}$ both in the field (in situ) and in the laboratory. In situ measurements usually deal with extremely low concentration of microorganisms and are designed to overcome this difficulty by increasing the path length of the sample. Some of these methods include:

- *Reflecting tube absorption meter*. This technique uses a tube with reflective walls as the sample holder [97,98]. The tube is illuminated with collimated monochromatic light at one end. As the light propagates through the sample it gets absorbed and scattered. The scattered light is reflected from walls and detected at the other end together with the transmitted light. The optical pathlength of the detected scattered light is larger than that of the transmitted light resulting in over estimation of the absorption coefficient.
- *Isotropic point source techniques*. This technique relies on the principle that irradiance from an isotropic point

source decays proportional to $\exp(-\kappa_{N,\lambda}R)/R^2$, where R is the radial distance from the source [99]. Thus, the absorption coefficient can be obtained by measuring the irradiance at different radial distances from the source. This method is valid for single scattering regime and enables the measurement of small absorption coefficients of natural waters.

Furthermore, some of the laboratory techniques for measuring the absorption coefficient include:

- *Integrating cavity absorption meter*. This technique uses a special sample holder known as the integrating cavity made of two concentric cavities separated by a diffuse translucent wall [100]. The sample is contained in the innermost cavity and is illuminated homogeneously from all directions with monochromatic light delivered by a set of fiber-optics. The attenuated light is detected by two sets of fiber-optics at two different radial locations with respect to the sample. The device is calibrated with Irgalan Black and Alcian Blue solutions of known absorption characteristics taking into account the geometry of the device. This device is regarded as one of the most accurate methods for measuring the absorption coefficient [93].
- *Photoacoustic technique*. In this technique, the sample is irradiated with a beam of light chopped at some arbitrary frequency [68]. The absorbed light is dissipated as heat causing periodic changes in sample temperature. These temperature changes give rise to pressure oscillations which can be detected by a microphone and correlated to the absorption coefficient of the particles [101].
- *Integrating sphere technique*. This method relies on the fact that microorganism suspensions scatter light strongly in the forward direction [69,96]. Thus, a significant portion of the scattered radiation is collected by the integrating sphere which has a large acceptance angle. Thus, the attenuation in the transmitted radiation is attributed solely to the effect of absorption. However, absorption coefficient obtained with this method suffers from scattering errors [72,102,103]. Several correction methods have been suggested by Davies-Colley [72], Merzlyak and Naqvi [104], and Stramski and Piskozub [103].

The integrating sphere technique is relatively easy to implement and is convenient for various microorganisms. Fig. 10a illustrates the experimental setup for determining the absorption coefficient $\kappa_{N,\lambda}$ of microorganisms suspensions from hemispherical transmittance of a suspension with cell density N denoted by $T_{h,\lambda,N}$ [96]. The microorganism suspension should be continuously flown through a flow cell to keep them randomly distributed and oriented and to avoid sedimentation. Under single scattering conditions, the apparent absorption coefficient $\chi_{h,\lambda}$ is related to the hemispherical transmittance $T_{h,\lambda,X}$ by [72],

$$\chi_{h,\lambda} = -\frac{1}{t}\ln\left(\frac{T_{h,\lambda,N}}{T_{h,\lambda,ref}}\right) \tag{25}$$

where $T_{h,\lambda,ref}$ is the normal-hemispherical transmittance of the reference solution alone (e.g., PBS). Due to the geometry of the experimental setup all the scattered radiation cannot be captured and measured by the integrating sphere. Thus, $\chi_{h,\lambda}$ overestimates the actual absorption coefficient $\kappa_{N,\lambda}$ which can be retrieved as [72]

$$\kappa_{N,\lambda} = \chi_{h,\lambda} - (1-\varepsilon_h)\sigma_{N,\lambda} \tag{26}$$

where ε_h is the fraction of scattered light detected by the integrating sphere. Ideally, ε_h is equal to unity when all light scattered in all directions is collected and detected by the integrating sphere. In order to correct for the scattering errors, Davies-Colley [72] assumed that the microorganisms do not absorb radiation at wavelength λ_o (e.g., $\lambda_o = 750$ nm for *A. variabilis* and $\lambda_o = 900$ nm for *R. sphaeroides* [62]). At this wavelength, the apparent absorption coefficient is equal to the scattering error given as

$$\chi_{h,\lambda_o} = (1-\varepsilon_h)\sigma_{N,\lambda_o} \tag{27}$$

Combining Eqs. (26) and (27) yields,

$$\kappa_{N,\lambda} = \chi_{h,\lambda} - \chi_{h,\lambda_o}\frac{\sigma_{N,\lambda}}{\sigma_{N,\lambda_o}} \quad \text{where} \quad \frac{\sigma_{N,\lambda}}{\sigma_{N,\lambda_o}} = \frac{\chi_\lambda - \chi_{h,\lambda}}{\chi_{\lambda_o} - \chi_{h,\lambda_o}} \tag{28}$$

Finally, to confirm that scattering is strongly forward, the hemispherical reflectance of the samples should be measured with an integrating sphere to evaluate the

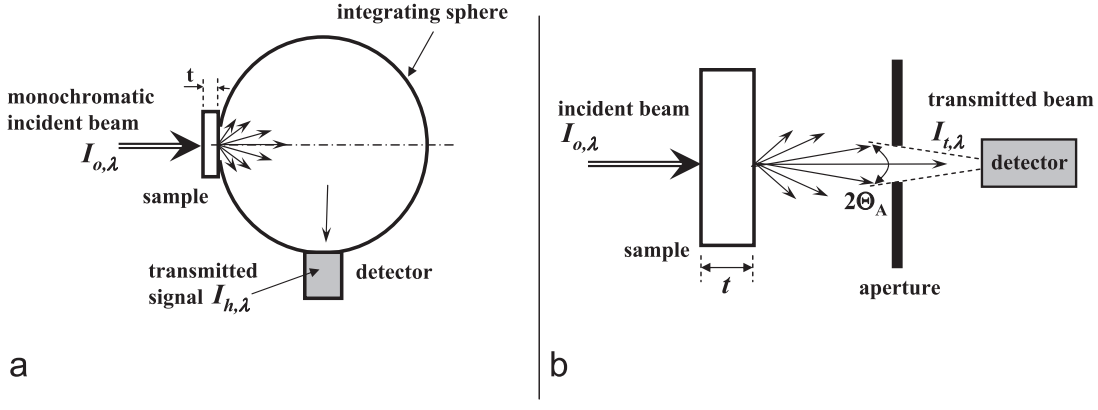

Fig. 10. Setup for determining (a) absorption coefficient $\kappa_{N,\lambda}$ from normal-hemispherical spectral transmittance and (b) the extinction coefficient $\beta_{N,\lambda}$ from normal–normal spectral transmittance.

contribution of backscattering to the overall attenuation of light by the microorganisms. If the hemispherical reflectance is only a few percent, then back-scattering can indeed be neglected in recovering the absorption coefficient $\kappa_{N,\lambda}$ using Eq. (25).

4.4. Extinction coefficient, $\beta_{N,\lambda}$

The extinction coefficient $\beta_{N,\lambda}$ can be measured from normal–normal transmittance measurements of dilute suspensions [68]. The most common technique uses a spectrometer where a collimated monochromatic beam is incident on a cuvette containing the suspension as illustrated in Fig. 10b. The transmitted light is focused onto a pinhole in front of the detector to eliminate the scattered light in directions other than the normal direction [94]. Here also, the microorganisms are continuously flown through a flow cell. In order to account for reflection and refraction by the cuvette, measurements are made with respect to the transmission spectrum of the reference medium alone in the cuvette denoted by $T_{n,\lambda,ref}$. Microorganism suspensions are known to scatter light strongly in the forward direction [69,96]. Therefore, care has to be taken to ensure that forward scattered radiation in directions other than the incident direction is eliminated in the measurement of the normal–normal transmittance $T_{n,\lambda,N}$ [68]. In fact, due to typical strongly forward scattering combined with large detector acceptance angle, the spectrometer measured an apparent extinction coefficient χ_λ given as [72,102],

$$\chi_\lambda = -\frac{1}{t}\ln\left(\frac{T_{n,\lambda,N}}{T_{n,\lambda,ref}}\right) \tag{29}$$

The apparent extinction coefficient is related to the absorption and extinction coefficients by [102,72],

$$\chi_\lambda = \kappa_{N,\lambda} + \sigma_{N,\lambda} - \varepsilon_n \sigma_{N,\lambda} \tag{30}$$

where ε_n represents the portion of the light scattered in the forward direction and detected by the spectrometer in directions other than the normal direction due to the finite size of the acceptance angle. It is defined as [105,91],

$$\varepsilon_n = \frac{1}{2}\int_0^{\Theta_a} \Phi_{N,\lambda}(\Theta)\sin\Theta\,\mathrm{d}\Theta \tag{31}$$

where Θ_a is the half acceptance angle of the detector. Using Eq. (30), the extinction coefficient can be determined as

$$\beta_{N,\lambda} = \kappa_{N,\lambda} + \sigma_{N,\lambda} = \frac{\chi_\lambda - \varepsilon_n \kappa_{N,\lambda}}{1-\varepsilon_n} \tag{32}$$

Bohren and Huffman [94] indicated that for reliable measurement of the extinction coefficient of highly forward scattering samples, the half acceptance angle of the detector Θ_a has to satisfy $\Theta_a < 1/2x_\lambda$ where x_λ is the size parameter defined as $x_\lambda = 2\pi a n_\lambda/\lambda$. Here, a is the scattering particle radius, n_λ is the refractive index of the non-absorbing and non-scattering medium in which the particles are submerged.

Alternatively, Privoznik et al. [96] measured the extinction coefficient of unicellular green algae *C. pyrenoidosa* using a nephelometer described in Section 4.2. Here, the fiber-optic probe submerged in the microorganism suspension thus, eliminating possible reflection and refraction by the container walls. Then, the radiation flux $F_\lambda(z)$ in the forward direction ($\Theta = 0^o$), expressed in Wm^{-2}, at two different locations z_1 and z_2 along the path of a divergent incident beam are measured (see Fig. 9). The extinction coefficient can be evaluated as [96]

$$\beta_{N,\lambda} = \frac{\ln|F_\lambda(z_2)/F_\lambda(z_1)| + \ln|z_1^2/z_2^2|}{z_1 - z_2} \tag{33}$$

where z is the distance between the detector and the virtual image of the last lens in the optical setup shown in Fig. 9b. Note that the second term in the numerator accounts for the divergence of the incident beam. Finally, the scattering coefficient can be computed as $\sigma_{N,\lambda} = \beta_{N,\lambda} - \kappa_{N,\lambda}$.

4.5. Validation

The experimental setups and analysis for measuring $\Phi_{N,\lambda}(\hat{s}_i,\hat{s})$, $\kappa_{N,\lambda}$ and $\beta_{N,\lambda}$ should be validated with monodisperse microspheres (e.g., SiO_2 or polystyrene Latex) of known diameter and randomly oriented fibers long enough to be treated as infinitely long. Experimental results can then be compared with those predicted from Mie theory for spheres [94] and for infinitely long and randomly oriented cylinders [106].

4.6. Example: radiation characteristics of C. littorale

For illustration purposes, Fig. 11a–c shows the spectral absorption $A_{abs,\lambda}$, extinction $E_{ext,\lambda}$, and scattering $S_{sca,\lambda}$ cross-sections of *C. littorale* measured at three different concentrations N, namely 3.2624×10^{11}, 3.6708×10^{11}, and 4.8106×10^{11} cells/m^3 in the spectral region from 400 to 800 nm [107]. First, it establishes that (i) the cross-sections $A_{abs,\lambda}$, $E_{ext,\lambda}$, and $S_{sca,\lambda}$ are independent of concentration N and (ii) scattering dominates over absorption at all wavelengths between 400 and 800 nm. In addition, the absorption peaks observed at 435 and 676 nm correspond to the absorption peaks of in vivo chlorophyll *a* [39]. In addition, in vivo chlorophyll *b* has absorption peaks at 475 and 650 nm [39] (Fig. 6). Thus, the absorption peak at 475 nm and the peak broadening around 650 nm observed in Fig. 11a can be attributed to the presence of chlorophyll *b*. Finally, Fig. 11d shows the scattering phase function of *C. littorale* measured with a nephelometer at 632.8 nm along with the Henyey–Greenstein scattering phase function $g_{N,\lambda} = 0.97$. It is evident that this microorganism is strongly forward scattering.

Moreover, Berberoğlu and co-workers [62,63] experimentally measured the radiation characteristics of several H_2 producing microorganisms namely (a) purple non-sulfur bacteria *R. sphaeroides* [62], (b) cyanobacteria *A. variabilis* [62], and (c) green algae *C. reinhardtii* strain CC125 and its truncated chlorophyll antenna transformants *tla1*, *tlaX*, and *tla1-CW*$^+$ [63], as well as (iii) the lipid producing microalgae *B. brauni* and *C. sp.* [107]. It was established that *R. sphaeroides* absorbs mainly in two distinct spectral regions from 300 to 600 nm and from 750 to 900 nm. The major absorption peaks can be observed around 370, 480, 790, and 850 nm and can be attributed to the presence of bacteriophyll b and carotenoids in the antenna complexes B850 and the reaction center complex [38,108]. Moreover, *A. variabilis* and the

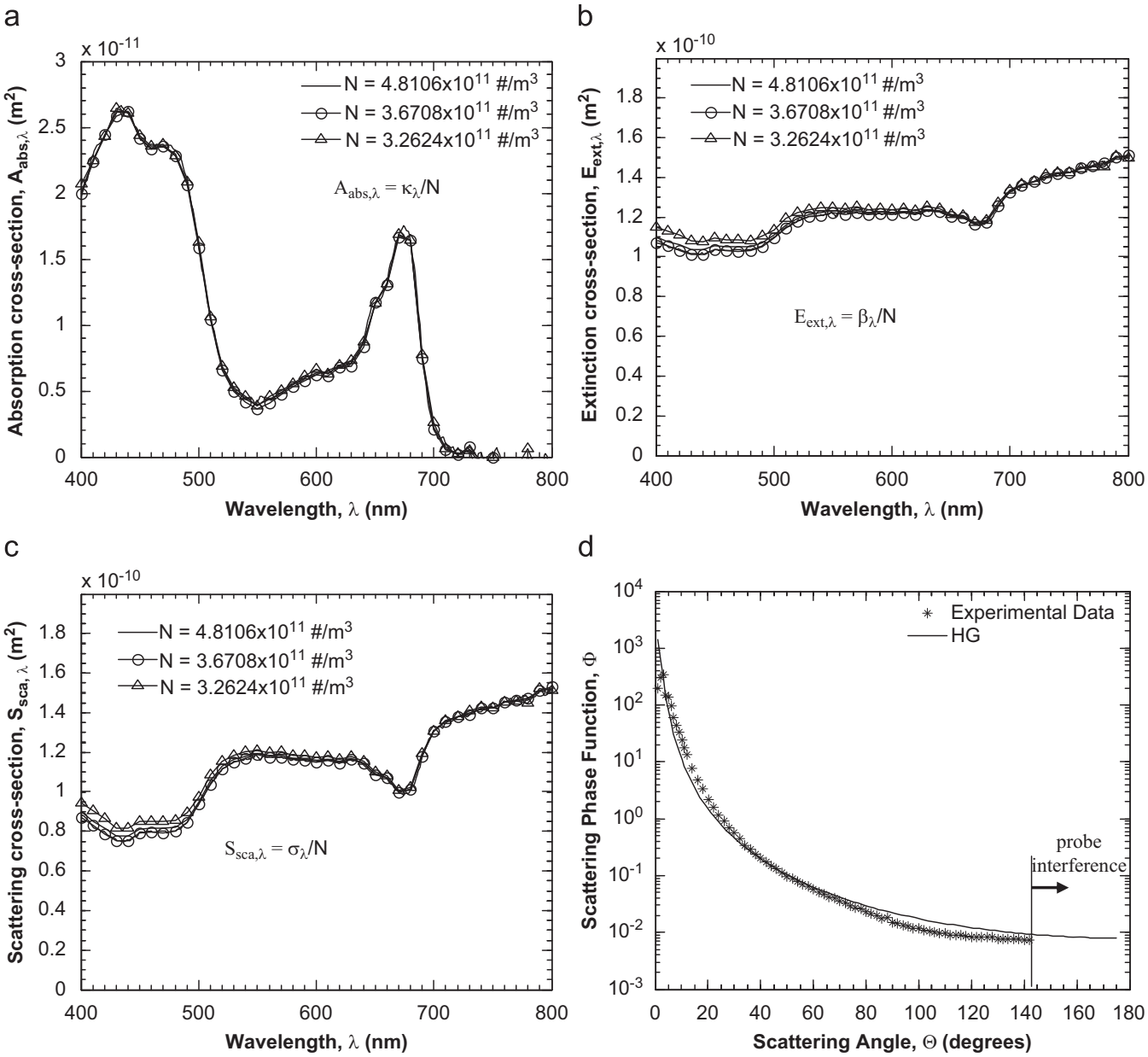

Fig. 11. The (a) absorption $A_{abs,\lambda}$, (b) extinction $E_{ext,\lambda}$, (c) scattering $S_{sca,\lambda}$ cross-sections over the spectral range from 400 to 800 nm for three different microorganism concentrations and (d) scattering phase function at 632.8 nm of *C. littorale* [107].

wild strain *C. reinhardtii* CC125 absorb mainly in the spectral region from 300 to 700 nm with absorption peaks at 435 and 676 nm corresponding to in vivo absorption peaks of chlorophyll *a*. *A. variabilis* also absorbs at 621 nm corresponding to absorption by the pigment phycocyanin [38] while *C. reinhardtii* has additional absorption peaks at 475 and 650 nm corresponding to absorption by chlorophyll *b*. The data collected in the above studies are available in digital form online [109] or directly from the corresponding author upon request.

5. Strategies to overcome light transfer limitations

Several strategies are being pursued to increase the efficiency of photobiological lipid or hydrogen production. First, with the advent of genetic engineering, microorganisms can be engineered to have the desired pigment concentrations. Second, processes and photobioreactors can be designed to increase efficiency by achieving optimum light delivery and maximizing sunlight utilization.

5.1. Truncating the light harvesting antenna

Microorganisms that are found in nature are not always subjected to optimum illumination. Therefore, as a survival mechanism they have adapted to produce relatively large amounts of pigments. This maximizes the probability of capturing and utilizing photons at low light intensities. However, when these microorganisms are mass cultured in photobioreactors, they absorb more photons than they can utilize and waste the light energy as heat and fluorescence [33]. The emitted fluorescent light can be absorbed by the suspension. However, the fluorescence quantum yield, defined as the ratio of the

number of photons emitted by fluorescence to the number of photons absorbed, is typically a few percent [110]. In addition, light does not penetrate deep into the photobioreactor. Thus, the quantum efficiency of photobiological fuel production decreases. Moreover, high intensities can catalyze formation of harmful oxides that can damage the photosynthetic apparatus, a process known as photo-oxidation [39]. Therefore, it is desirable to decrease the chlorophyll antenna size down to the size of the core antenna [111].

Melis et al. [33,112] physiologically reduced the pigment content of the green algae *Dunaliella salina* from 1×10^9 chlorophyll molecules per cell (Chl/cell) to 0.15×10^9 Chl/cell. More recently, Polle et al. [111] genetically engineered the green algae *C. reinhardtii* with truncated light harvesting chlorophyll antenna size. The authors reported that the microorganisms with less pigments had higher quantum yield, photosynthesis rate, and saturation fluence rate [111].

Fig. 12 shows the in vivo differential interference contrast (DIC) and chlorophyll fluorescence micrographs of green algae *C. reinhardtii* CC125 and its truncated chlorophyll antenna transformants *tla1*, *tlaX*, and *tla1*-CW$^+$ [63]. It was obtained with a confocal scanning laser microscope in the transmission and epi-fluorescence mode simultaneously at excitation wavelength of 543 nm and fluorescence emission above 560 nm [63]. The figure illustrates the size and shape of each strain as well as the location of the chlorophyll pigments which fluoresce in red [40]. The strong red fluorescence observed in the wild strain CC125 qualitatively shows that it has the highest concentration of chlorophyll while *tlaX* has the lowest.

Fig. 13 shows the absorption and scattering cross-sections of wild and genetically engineered strains of *C. reinhardtii* between 350 and 750 nm [63]. It is evident that genetically engineered strains have significantly smaller absorption cross-sections than the wild strain. This is particularly true of the mutant *tlaX* due to their smaller chlorophyll *b* content. For all mutants, however, the reduction in the absorption cross-section is accompanied by an increase in scattering cross-section [63]. Although scattering becomes the dominant phenomenon contributing to the overall extinction of light, it is mainly in the forward direction so light penetrates within the reactor.

5.2. Process optimization

Several processes have been considered to further develop photobiological fuel production technologies including controlled and optimum light delivery and mixed or symbiotic cultures of different types of microorganisms.

5.2.1. Advanced light delivery system

The saturation fluence rate of photosynthetic apparatus is on the order of 5000–6000 lux [113]. This corresponds to about one tenth of the total solar irradiance where the rest of the energy is wasted as heat and fluorescence. Thus, light can be delivered to 10 times larger surface area using solar collectors and lightguides to enhance the solar energy utilization efficiency. To do so, cost effective light delivery technologies need to be developed and integrated into the design of future photobioreactors.

The simplest solution is to divide the incident solar radiation and deliver it on two sides of a flat panel PBR instead of on a single side. In fact, Rodolfi et al. [114] reported that two-side illumination resulted in greater lipid productions and efficiency than one-side illumination with twice the incident irradiance to ensure that the same amount of energy was delivered.

Moreover, system engineers are designing novel photobioreactors that collect and deliver sunlight in a controlled

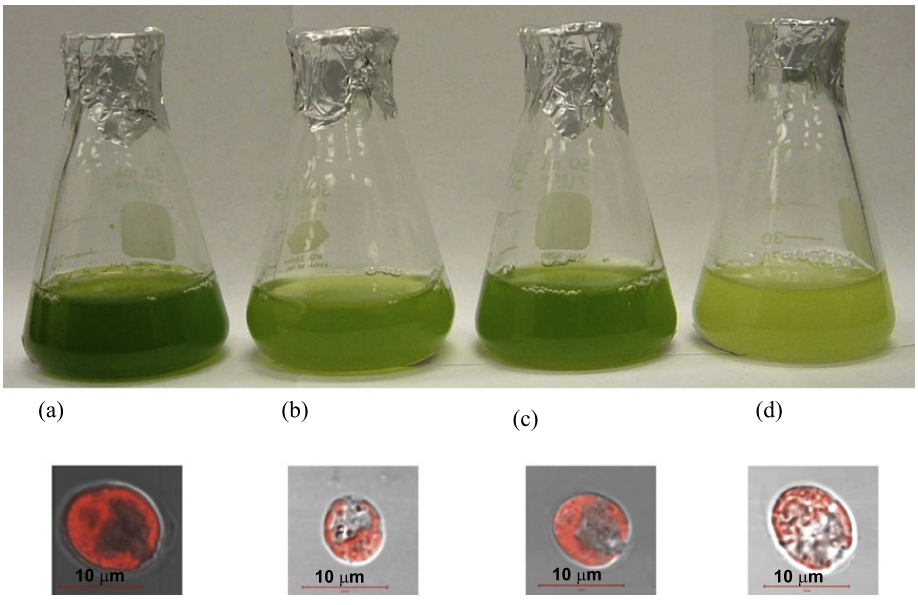

Fig. 12. (top) Photograph of flasks containing suspensions of the same concentration of *C. reinhardtii* (a) CC125, (b) *tla1*, (c) *tlaX*, and *tla1*-CW$^+$ and (bottom). Differential interference contrast and fluorescence micrographs of these green algae [63]. The scale bars correspond to 10 μm.

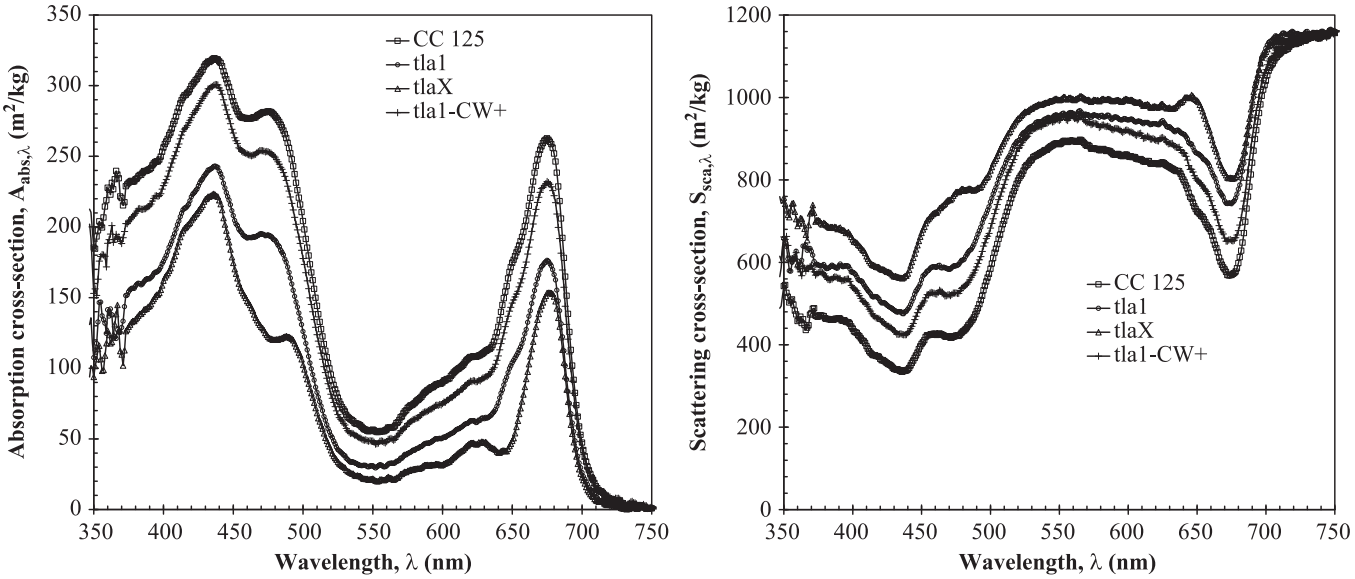

Fig. 13. Absorption and scattering cross-sections of the green algae *C. reinhardtii* CC 125 and its truncated chlorophyll antenna transformants *tla1*, *tlaX*, and *tla1-CW*$^+$ [63].

manner within the photobioreactor [16,17,115–118]. These systems usually involve a heliostat composed of either fresnel lenses [17] or reflective dishes [115,116] that concentrate the solar radiation to be distributed via fiber optics or lightguides. The lightguides are made of glass or acrylic and can deliver sunlight deep into the photobioreactors by total internal reflection. At desired locations, the lightguides have rough surfaces and light "leaks" out providing the desired irradiance. For example, Fig. 14 shows a light delivery apparatus immersed in water featuring alternatively smooth and rough surfaces. Light is guided in the rod whose refractive index (n_1) is larger than that of the surrounding liquid medium ($n_2 < n_1$). The transparent rod can be made of glass or plexiglass. As the incident light is guided along the rod, it remains inside the rod as long as the angle of incidence at the rod/liquid interface remains larger than the critical angle for total internal reflection given by $\theta_c = \sin^{-1}(n_2/n_1)$. By adjusting the roughness profile the desired light delivery can be achieved. Note that the same principle applies to fiber optics which can also be used to deliver light inside PBRs.

In some elaborate designs, light emitting diodes (LEDs) are also incorporated into the lightguide delivery system to provide artificial light to the microorganisms at night [119]. Lightguides and fiber optics have been used to increase the light irradiance in the center of photobioreactors where it is typically the lowest [118]. However, this technology is judged too costly to be adopted at industrial scale [30].

Alternatively, Kondo et al. [30] proposed the culture of two types of photosynthetic bacteria namely *R. sphaeroides* RV and its reduced-pigment mutant MTP4 in two separate but adjacent plate-type photobioreactors. MTP4 produces H_2 more efficiently under high irradiance while *R. sphaeroides* RV is more efficient under low irradiance. The authors showed that two plate-type photobioreactors with MTP4 in the front reactor and *R. sphaeroides* RV in the rear reactor illuminated on one side produced more than if either species were alone in both reactors. In other words, the front reactor acted as a absorption filter to the second.

5.2.2. Mixed cultures

To date, majority of research efforts have concentrated on cultivating single species of microogranisms for photobiological fuel production. Among these, cyanobacteria and green algae which utilize solar energy in the spectral range from 400 to 700 nm to produce hydrogen have been studied extensively [120]. On the other hand, purple non-sulphur bacteria have also been identified as potential hydrogen producers which mainly use solar energy in the near-infrared part of the spectrum from 700 to 900 nm [84]. Note that only about 45% of the total solar radiation is emitted between 400 and 700 nm and an additional 20% is emitted between 700 and 900 nm [121].

Thus, mixed cultivation of green algae and purple bacteria has the potential to achieve higher solar to hydrogen energy conversion efficiencies than single cultures by using solar radiation in the spectral range from 400 to 900 nm where 65% of the total solar radiation is concentrated. Such a mixed culture has been demonstrated by Melis and Melnicki [121] where the green algae *C. reinhardtii* were co-cultured with the purple bacteria *R. rubrum*. The authors suggested that once the photosynthesis to respiration (P/R) ratio of the green algae is reduced to 1, such a co-culture could be used for more efficient photobiological hydrogen production. Currently, the wild strain algae have a P/R of about 4 [121]. Unfortunately, the purple bacteria also absorb light in the visible part of the spectrum due to the presence of bacteriochlorophyll b and carotenoids [62]. Consequently, the two species may compete for light during both the growth and the hydrogen production phases.

Recently, Berberoğlu and Pilon [83] reported a numerical study aiming to maximize the solar to hydrogen energy conversion efficiency of a mixed culture

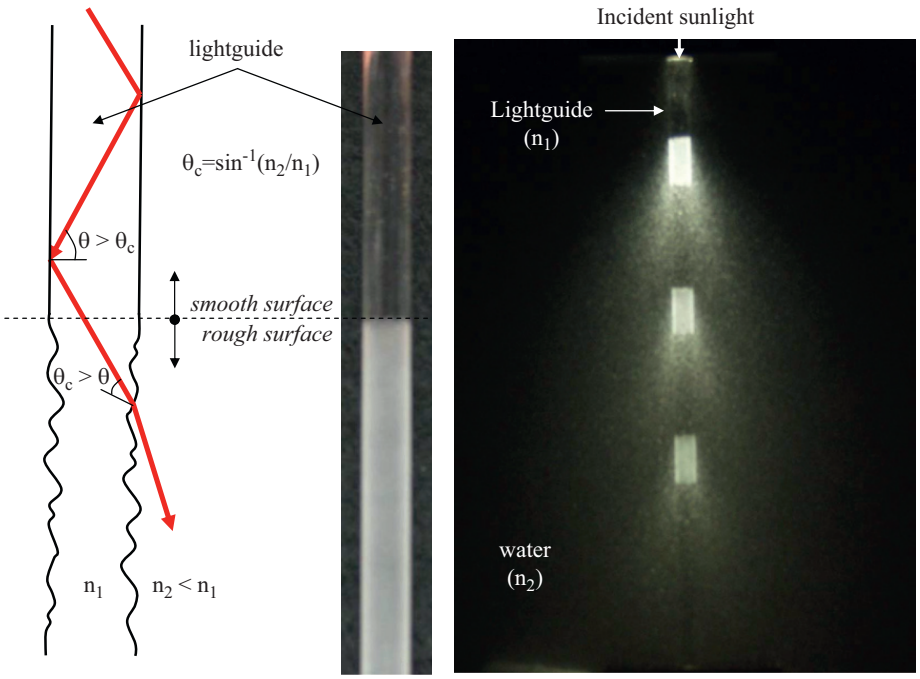

Fig. 14. Principle and demonstration of lightguide 6.4 mm in diameter with alternatively rough sections separated by 2.54 cm long smooth regions for controlled light delivered at desired depths inside a photobioreactor. (Experiments performed at UCLA by E. Wostenberg, unpublished data).

containing the green algae *C. reinhardtii* and the purple non-sulfur bacteria *R. sphearoides*. The authors used the radiation characteristics they had measured experimentally [62,63] as input parameters for calculating the local spectral incident radiation within a flat panel photobioreactor. Their results show that for monocultures, the solar to H_2 energy conversion efficiency depends only on the optical thickness of the system. The maximum solar energy conversion efficiency of mono-cultures of *C. reinhardtii* and *R. spaheroides*, considering the entire solar spectrum, was found to be 0.061 and 0.054%, respectively, corresponding to optical thicknesses of 200 and 16, respectively. Using mixed cultures, a total conversion efficiency of about 0.075% could be achieved corresponding to an increase of about 23% with respect to that of a monoculture of *C. reinhardtii*. The choice of microorganism concentrations for maximum solar energy conversion efficiency in mixed cultures was non-trivial and requires careful radiation transfer analysis coupled with H_2 production kinetics.

5.2.3. Symbiotic cultures

Another strategy to increase efficiency of photobioreactors is to grow symbiotic cultures such as combining purple non-sulfur bacteria and anaerobic fermentative bacteria. For example, Miyake et al. [122] used symbiotic cultures of the anaerobic fermentative bacteria *Clostridium butyricum* and the purple non-sulfur bacteria *R. sphaeroides* to produce H_2. In this symbiotic culture, the anaerobic bacteria converted sugars to H_2 and organic acids, whereas the purple non-sulfur bacteria converted the organic acids produced by the other species into H_2. Overall, their symbiotic system produced 7 mol of H_2 per mole of glucose.

6. Conclusion

This review presented the current state of knowledge in radiation transfer in solar to fuel conversion as well as CO_2 fixation using photosynthetic microorganisms. It provided the reader with a basic background on photosynthesis and photobiological lipid and H_2 production. Then, modeling of radiation transfer in photobioreactors was described. Strategies to overcome light limitation and optimize light delivery were discussed. In brief, photobiological liquid fuel or H_2 production is at relatively early stage of their development and requires additional basic and applied research efforts. However, progresses from genetic engineering to innovative photobioreactor designs with advanced light delivery are promising. If successful, this technology will offer a long term solution for sustainable fuel production. It will also alleviate concerns over energy security with the advantage of capturing CO_2 responsible for global warming [3].

References

[1] International Energy Agency, Key World Energy Statistics 2007, 〈http://www.iea.org/Textbase/stats/index.asp〉; 2007.
[2] Energy Information Administration, International energy outlook 2008—highlights, Report DOE/EIA-0484, June 2008.
[3] IPPC, Climate change 2007: Impacts, adaptation and vulnerability. contribution of working group ii to the fourth assessment report of the intergovernmental panel on climate change. Cambridge, UK: Cambridge University Press; 2007.
[4] U.S. Central Intelligence Agency, The World Factbook 2008, 〈https://www.cia.gov/cia/publications/factbook/index.html〉; 2008.
[5] Yamasaki A. An overview of CO_2 mitigation options for global warming—emphasizing CO_2 sequestration options. Journal of Chemical Engineering of Japan 2003;34:361–75.
[6] Peters W, Jacobson AR, Sweeney C, Andrews AE, Conway TJ, Masarie L, et al. An atmospheric perspective on North American

carbon dioxide exchange: carbon tracker. Proceedings of the National Academy of Science 2007;27(48):18925–30.
[7] Liou KN. An introduction to atmospheric radiation. 2nd ed. San Diego, CA: Academic Press; 2002.
[8] Duffie JA, Beckman WA. Solar engineering of thermal processes. 3rd ed. Hoboken, New Jersey: John Wiley and Sons; 2006.
[9] Gueymard C, Myers D, Emery K. Proposed reference irradiance spectra for solar energy systems testing. Solar Energy 2002;73(6): 443–67.
[10] The National Oceanic and Atmospheric Administration (NOAA), US standard atmosphere, 1976, Technical Report NOAA/NASA/USAF - NOAA-S/T76-1562, Washington, DC; 1976.
[11] Gueymard C. SMARTS Code, Version 2.9.2 User's direct beam spectral irradiance data for photovoltaic cell Manual, Solar Consulting Services, 〈http://rredc.nrel.gov/solar/models/SMARTS〉; 2002.
[12] SunWize Technologies, World insolation map, 〈http://www.sunwize.com/info_center/solar-insolation-map.php〉; 2008.
[13] Bolton JR, Hall DO. The maximum efficiency of photosynthesis. Photochemistry and Photobiology 1991;53:545–8.
[14] Sheehan J, Dunahay T, Benemann J, Roessler P. A look back at the U.S. Department of Energy's aquatic species program—biodiesel from algae, Technical Report NREL/TP-580-24190; 1998.
[15] Chelf P, Brown LM, Wyman CE. Aquatic biomass resources and carbon dioxide trapping. Biomass and Bioenergy 1993;4(3): 175–83.
[16] Stewart C, Hessami MA. A study of methods of carbon dioxide capture and sequestration—the sustainability of a photosynthetic bioreactor approach. Energy Conversion and Management 2005;46(3):403–20.
[17] Hirata S, Hayashitani M, Taya M, Tone S. Carbon dioxide fixation in batch culture of *Chlorella sp.* using a photobioreactor with a sunlight-collection device. Journal of Fermentation and Bioengineering 1996;81(5):470–2.
[18] Keffer JE, Kleinheinz GT. Use of *Chlorella vulgaris* for CO_2 mitigation in a photobioreactor. Journal of Industrial Microbiology and Biotechnology 2002;29:275–80.
[19] Yoon JH, Sim SJ, Kim MS, Park TH. High cell density culture of *Anabaena variabilis* using repeated injections of carbon dioxide for the production of hydrogen. International Journal of Hydrogen Energy 2002;27(11–12):1265–70.
[20] Vunjak-Novakovic G, Kim Y, Wu XX, Berzin I, Merchuk JC. Air-lift bioreactors for algal growth on flue gas: Mathematical modeling and pilot-plant studies. Industrial and Engineering Chemistry Research 2005;44(16):6154–63.
[21] Skjånes K, Lindblad P, Muller J. BioCO_2—a multidisciplinary, biological approach using solar energy to capture CO_2 while producing H_2 and high value products. Biomolecular Engineering 2007;24(4):405–13.
[22] Hall DO, Markov SA, Watanabe Y, Rao KK. The potential applications of cyanobacterial photosynthesis for clean technologies. Photosynthesis Research 1995;46(1–2):159–67.
[23] Lundquist TJ, Woertz IC, Quinn NWT, Benemann JR. A realistic technology and engineering assessment of algae biofuel production, Technical Report, Energy Biosciences Institute, University of California, Berkeley; 2010.
[24] Davis R, Aden A, Pienkos PT. Techno-economic analysis of autotrophic microalgae for fuel production. Applied Energy 2001;88(10):3524–31.
[25] Jorquera O, Kiperstok A, Sales E, Embirucu M, Ghirardi M. Comparative energy life-cycle analyses of microalgal biomass production in open ponds and photobioreactors. Bioresource Technology 2010;101:1406–13.
[26] Pate R, Klise G, Wu B. Resource demand implications for us algae biofuels production scale-up. Applied Energy 2011;88:3377–88.
[27] Wigmosta MS, Coleman AM, Skaggs RJ, Huesemann MH, Lane LJ. National microalgae biofuel production potential and resource demand. Water Resources Research 2011;47:1–13.
[28] Pulz O. Photobioreactors: production systems for phototrophic microorganisms. Applied Microbiology and Biotechnology 2001;57(3):287–93.
[29] Benemann JR. Hydrogen production by microalgae. Journal of Applied Phycology 2000;12(3–5):291–300.
[30] Kondo T, Arakawa M, Wakayama T, Miyake J. Hydrogen production by combining two types of photosynthetic bacteria with different characteristics. International Journal of Hydrogen Energy 2002;27(11–12):1303–8.
[31] Ogbonna JC, Soejima T, Tanaka H. An integrated solar and artificial light system for internal illumination of photobioreactors. Journal of Biotechnology 1999;70(1–3).
[32] Lee J-S, Lee J-P. Review of advances in biological CO_2 mitigation technology. Biotechnology and Bioprocess Engineering 2003;8(6): 354–9.
[33] Melis A, Neidhardt J, Benemann JR. *Dunaliella salina* (*Chlorophyta*) with small chlorophyll antenna sizes exhibit higher photosynthetic productivities and photon use efficiencies than normally pigmented cells. Journal of Applied Phycology 1999;10(6):515–25.
[34] Gueymard CA, Myers D, Emery K. Proposed reference irradiance spectra for solar energy system testing. Solar Energy 2002;73(6): 443–67.
[35] Cornet JF, Dussap CG, Dubertret G. A structured model for simulation of cultures of the cyanobacterium *Spirulina platensis* in photobioreactors: I. Coupling between light transfer and growth kinetics. Biotechnology and Bioengineering 1992;40(7):817–25.
[36] Cornet JF, Dussap CG, Cluzel P, Dubertret G. A structured model for simulation of cultures of the cyanobacterium *Spirulina platensis* in photobioreactors: II. Identification of kinetic parameters under light and mineral limitations. Biotechnology and Bioengineering 1992;40(7):826–34.
[37] Cornet JF, Dussap CG, Gross JB, Binois C, Lasseur C. A simplified monodimensional approach for modeling coupling between radiant light transfer and growth kinetics in photobioreactors. Chemical Engineering Science 1995;50(9):1489–500.
[38] Madigan MT, Martinko JM. Biology of microorganisms. Upper Saddle River, NJ: Pearson Prentice Hall; 2006.
[39] Ke B, Photosynthesis. Photobiochemistry and photobiophysics. Dordrecht, The Netherlands: Kluwer Academic Publishers; 2001.
[40] Harris EH. The *Chlamydomonas* sourcebook—volume 1. San Diego, CA: Academic Press; 1989.
[41] Hu Q, Sommerfeld M, Jarvis E, Ghirardi M, Posewitz M, Seibert M, et al. Microbial triacylglycerols as feedstocks for biofuel production: perspectives and advances. The Plant Journal 2008;54: 621–39.
[42] Chisti Y. Biodiesel from algae. Biotechnology Advances 2007;25: 294–306.
[43] Ohlrogge J, Browse J. Lipid biosynthesis. Plant Cell 1995;7:957–70.
[44] Ratledge C. An overview of microbial lipids. In: Ratledge C, Wilkerson SG, editors. In microbial lipids, vol. 1. New York, NY: Academic Press; 1988.
[45] Reitan KI, Rainuzzo JR, Olsen Y. Stimulation of hydrogen production in algae by removal of oxygen by reagents that combine reversibly with oxygen. Journal of Phycology 1994;30:972–9.
[46] Roessler PG. Changes in the activities of various lipid and carbohydrate biosynthetic enzymes in the diatom *Cyclotella cryptica* in response to silicon deficiency. Archives of Biochemistry and Biophysics 1988;267:521–8.
[47] Basova MM. Fatty acid composition of lipids in microalgae. International Journal on Algae 2005;7:33–57.
[48] Lynch DV, Thompson GA. Low temperature-induced alterations in the chloroplast and microsomal membranes of *Dunaliella salina*. Plant Physiology 1982;69:1369–75.
[49] Renaud SM, Thinh LV, Lambrinidis G, Parry DL. Effect of temperature on growth, chemical composition and fatty acid composition of tropical Australian microalgae grown in batch cultures. Aquaculture 2002;211:195–214.
[50] Brown MR, Dunstan GA, Norwood SJ, Miller KA. Effects of harvest stage and light on the biochemical composition of the diatom *Thalassiosira pseudonana*. Journal of Phycology 1996;32:64–73.
[51] Khotimchenko SV, Yakovleva IM. Lipid composition of the red alga *Tichocarpus crinitus* exposed to different levels of photon irradiance. Phytochemistry 2005;66:73–9.
[52] Napolitano GE. The relationship of lipids with light and chlorophyll measurement in freshwater algae and periphyton. Journal of Phycology 1994;30:943–50.
[53] Spoehr HA, Milner HW. The chemical composition of *Chlorella*; effect of environmental conditions. Plant Physiology 1949;24: 120–49.
[54] Sukenik A, Yamaguchi Y, Livne A. Alterations in lipid molecular species of the marine eustigmatophyte *Nannochloropsis sp*. Journal of Phycology 1993;29:620–6.
[55] Orcutt DM, Patterson GW. Effect of light intensity upon *Nitzchia closternium* (*Cylindrotheca fusiformis*). Lipids 1974;9:1000–3.
[56] Pilon L, Berberoglu H. Photobiological hydrogen production. Boca Raton, FL: CRC Press, Taylor and Francis; 2011 ISBN-13: 978-1420054477.
[57] Das D, Veziroğlu TN. Hydrogen production by biological processes: a survey of literature. International Journal of Hydrogen Energy 2001;26(1):13–28.

[58] Prince RC, Kheshgi HS. The photobiological production of hydrogen: potential efficiency and effectiveness as a renewable fuel. Critical Reviews in Microbiology 2005;31(1):19–31.

[59] Hallenbeck PC, Benemann JR. Biological hydrogen production: fundamentals and limiting processes. International Journal of Hydrogen Energy 2002;27(11–12):1185–93.

[60] Pinto FAL, Troshina O, Lindblad P. A brief look at three decades of research on cyanobacterial hydrogen evolution. International Journal of Hydrogen Energy 2002;27(11–12):1209–15.

[61] Kapdan IK, Kargi F. Bio-hydrogen production from waste materials. Enzyme and Microbial Technology 2006;38(5):569–82.

[62] Berberoğlu H, Pilon L. Experimental measurement of the radiation characteristics of *Anabaena variabilis* ATCC 29413-U and *Rhodobacter sphaeroides* ATCC 49419. International Journal of Hydrogen Energy 2007;32(18):4772–85.

[63] Berberoğlu H, Melis A, Pilon L. Radiation characteristics of *Chlamydomonas reinhardtii* CC125 and its truncated chlorophyll antenna transformants *tla1*, and *tla1-CW*$^{+}$. International Journal of Hydrogen Energy 2008;33(22):6467–83.

[64] Hale GM, Querry MR. Optical constants of water in the 200-nm to 200-μm wavelength region. Applied Optics 1973;12:555563.

[65] Asenjo JA, Merchuk JC. Bioreactor system design. New York, NY: Marcel Dekker; 1995.

[66] Pulz O, Scheibenbogen K. Photobioreactors: design and performance with respect to energy input light. Advances in Biochemical Engineering/Biotechnology 1998;59:123–52.

[67] Suh IS, Lee CG. Photobioreactor engineering: design and performance. Biotechnology and Bioprocess Engineering 2003;8(6):313–21.

[68] Modest MF. Radiative heat transfer. San Diego, CA: Academic Press; 2003.

[69] Berberoğlu H, Yin J, Pilon L. Simulating light transfer in a bubble sparged photobioreactor for simultaneous hydrogen fuel production and CO_2 mitigation. International Journal of Hydrogen Energy 2007;32(13):2273–85.

[70] Mie G. Beiträge zur Optik trüber Medien, speziell kolloidaler Metallösungen. Annalen der Physik 1908;25(3):377–445.

[71] Stramski D, Mobley CD. Effect of microbial particles on oceanic optics: a database of single-particle optical properties. Limnology and Oceanography 1997;42:538–49.

[72] Davies-Colley RJ, Pridmore RD, Hewitt JE. Optical properties and reflectance spectra of 3 shallow lakes obtained from a spectrophotometric study. New Zealand Journal of Marine and Freshwater Research 1983;17:445–59.

[73] Bricaud A, Morel A, Prieur L. Optical efficiency factors of some phytoplankters. Limnology and Oceanography 1983;28:816–32.

[74] Lee SC, White S, Grzesik JA. Effective radiative properties of fibrous composites containing spherical particles. International Journal of Thermophysics and Heat Transfer 1994;8:400–5.

[75] Pottier L, Pruvost J, Deremetz J, Cornet JF, Legrand J, Dussap CG. A fully predictive model for one-dimensional light attenuation by *Chlamydomonas reinhardtii* in a torous photobioreactor. Biotechnology and Bioengineering 2005;91:569–82.

[76] Pruvost J, Legrand J, Legentilhomme P, Muller-Feuga A. Simulation of microalgae growth in limiting light conditions: flow effect. AIChE Journal 2002;48(5):1109–20.

[77] Acién Fernández FG, García Camacho F, Sánchez Pérez JA, Fernández Sevilla JM, Molina Grima E. A model for light distribution and average solar irradiance inside outdoor tubular photobioreactors for the microalgal mass culture. Biotechnology and Bioengineering 1997;55(5):701–14.

[78] Pruvost J, Cornet J-F, Legrand J. Hydrodynamics influence on light conversion in photobioreactors: an energetically consistent analysis. Chemical Engineering Science 2008;63(14):3679–94.

[79] Fouchard S, Pruvost J, Degrenne B, Legrand J. Investigation of H_2 production using the green microalga *Chlamydomonas reinhardtii* in a fully controlled photobioreactor fitted with on-line gas analysis. International Journal of Hydrogen Energy 2008;33(13):3302–10.

[80] Dunn IJ, Heinzle E, Ingham J, Prenosil JE. Biological reaction engineering: dynamic modelling fundamentals with simulation examples. 2nd ed.Wiley-VCH; 2003.

[81] Björkman O. Responses to different quantum flux densities. In: Lange OL, Nobel PS, Osmond CB, Zeigler H, editors. Encyclopedia of plant physiology, vol. 12A. Berlin, Germany: Springer; 1981. p. 57–107.

[82] Sorokin C, Krauss RW. The effects of light intensity on the growth rates of green algae. Plant Physiology 1958;33(2):109–13.

[83] Berberoğlu H, Pilon L. Maximizing solar to H_2 energy conversion efficiency of outdoor photobioreactors using mixed cultures. International Journal of Hydrogen Energy 2010;35:500–10.

[84] Nogi Y, Akiba T, Horikoshi K. Wavelength dependence of photoproduction of hydrogen by *Rhodopseudomonas rutila*. Agricultural and Biological Chemistry 1985;49:35–8.

[85] Erickson LE, Curless CE, Lee HY. Modeling and simulation of photosynthetic microbial growth. Annals of New York Academy of Sciences 1987;506:308–24.

[86] Wang C, Fu C, Liu Y. Effects of using light-emitting diodes on the cultivation of *Spirulina platensis*. Biochemical Engineering Journal 2007;37(1):21–5.

[87] Yeh N, Chung J. High-brightness LEDs-energy efficient lighting sources and their potential in indoor plant cultivation. Renewable and Sustainable Energy Reviews 2009;13(8):2175–80.

[88] Gordon J, Polle J. Ultrahigh bioproductivity from algae. Applied Microbiology and Biotechnology 2007;76:969–75.

[90] Bolton JR. Solar Photoproduction of Hydrogen, IEA Technical Report, IEA/H2/TR-96, 1996.

[91] Agrawal BM, Mengüç MP. Forward and inverse analysis of single and multiple scattering of collimated radiation in an axisymmetric system. International Journal of Heat and Mass Transfer 1991;34:633–47.

[92] Bohren CF. Multiple scattering of light and some of its observable consequences. American Journal of Physics 1986;55:524–33.

[93] Jonasz M, Fournier GR. Light scattering by particles in water: theoretical and experimental foundations. San Diego, CA: Academic Press; 2007.

[94] Bohren CF, Huffman DR. Absorption and scattering of light by small particles. New York: John Wiley & Sons; 1998.

[95] Daniel KJ, Laurendeau NM, Incropera FP. Prediction of radiation absorption and scattering in turbid water bodies. Journal of Heat Transfer 1979;101:63–7.

[96] Privoznik KG, Daniel KJ, Incropera FP. Absorption extinction and phase function measurements for algal suspensions of *Chlorella pyrenoidosa*. Journal of Quantitative Spectroscopy and Radiation Transfer 1978;20:345–52.

[97] Moore C, Seneveld RV, Kitchen JC. Preliminary results from an *in situ* spectral absorption meter. In: Ocean optics 11, proceedings of SPIE, vol. 1750; 1992. p. 330–7.

[98] Zaneveld JRV, Bartz R, Kitchen JC. Reflective tube absorption meter.

[99] Maffione RA, Voss KJ, Honey RC. Measurement of the spectral absorption coefficient in the ocean with an isotropic source. Applied Optics 1993;32:3273–9.

[100] Fry ES, Kattawar GW, Pope RM. Integrating cavity absorption meter. Applied Optics 1992;31:2055–65.

[101] Bennet GT, Fry ES, Sogandares FM. Photothermal measurements of the absorption coefficient of water at 590 nm. Ocean Optics 8, Proceedings of SPIE 1986;637:172–180.

[102] Davies-Colley RJ, Pridmore RD, Hewitt JE. Optical properties of some freshwater phytoplanktonic algae. Hydrobiologia 1986;133:165–78.

[103] Stramski D, Piskozub J. Estimation of scattering error in spectrophotometric measurements of light absorption by aquatic particles from three-dimensional radiative transfer simulations. Applied Optics 2003;42:3634–46.

[104] Merzlyak MN, Naqvi KR. On recording the true absorption spectrum and scattering spectrum of a turbid sample: application to cell suspensions of cyanobacterium *Anabaena variabilis*. Journal of Photochemistry and Photobiology B 2000;58:123–9.

[105] Kokhanovsky AA. Scattered light corrections to sun photometry: analytical results for single and multiple scattering regimes. Journal of Optical Society of America A 2007;24:1131–7.

[106] Lee SC. Scattering phase function for fibrous media. International Journal of Heat and Mass Transfer 1990;33:2183–90.

[107] Berberoğlu H, Gomez PS, Pilon L. Radiation characteristics of *Botryococcus braunii*, *Chlorococcum littorale*, and *Chlorella sp* used for CO_2 fixation and biofuel production. Journal of Quantitative Spectroscopy and Radiative Transfer 2009;110:1879–93.

[108] Broglie RM, Hunter CN, Delepelaire P, Niederman RA, Chua NH, Clayton RK. Isolation and characterization of the pigment–protein complexes of *Rhodopseudomonas sphaeroides* by lithium dodecylsulfate/polyacrylamide gel electrophoresis. Proceedings of the National Academy of Sciences of the United States of America 1980;77(1):87–91.

[109] Pilon L. Data and program downloads, 〈http://www.seas.ucla.edu/~pilon/downloads.htm〉; 2011.

[110] Maritorena S, Morel A, Gentili B. Determination of the fluorescence quantum yield by oceanic phytoplankton in their natural habitat. Applied Optics 2000;39(36):6725–37.
[111] Polle JE, Kanakagiri SD, Melis A. tla1, a DNA insertional transformant of the green alga *Chlamydomonas reinhardtii* with a truncated light-harvesting chlorophyll antenna size. Planta 2003;217(1):49–59.
[112] Melis A, Happe T. Trails of green alga hydrogen research—from Hans Gaffron to new frontiers. Photosynthesis Research 2004;80(1–3):401–9.
[113] Berberoğlu H, Jay J, Pilon L. Effect of nutrient media on photobiological hydrogen production by *Anabaena variabilis* ATCC 29413. International Journal of Hydrogen Energy 2008;33(3):1172–84.
[114] Rodolfi L, Chini Zittelli G, Bassi N, Padovani G, Biondi N, Bonini G, Tredici MR. Microalgae for oil: strain selection, induction of lipid synthesis and outdoor mass cultivation in a low-cost photobioreactor. Biotechnology and Bioengineering 2009;102(1):100–12.
[115] Bayless DJ, Kremer G, Vis M, Stuart B, Shi L, Cuello J, Ono E. Photosynthetic CO_2 mitigation using a novel membrane-based photobioreactor. Journal of Environmental Engineering and Management 2006;16(4):209–15.
[116] Akkerman I, Jansen M, Rocha J, Wijffels RH. Photobiological hydrogen production: photochemical efficiency and bioreactor design. International Journal of Hydrogen Energy 2002;27:1195–208.
[117] El-Shishtawy RMA, Kawasaki S, Morimoto M. Biological H_2 production using a novel light-induced and diffused photobioreactor. Biotechnology Techniques 1997;11(6):403–7.
[118] Chen CY, Lee CM, Chang JS. Hydrogen production by indigenous photosynthetic bacterium *Rhodopseudomonas palustris* WP3-5 using optical fiber-illuminating photobioreactors. Biotechnology Engineering Journal 2006;32(1):33–42.
[119] Ono E, Cuello JL. Design parameters of solar concentrating systems for CO_2 mitigating algal photobioreactors. Energy 2004;29(9–10):1651–7.
[120] Melis A, Happe T. Hydrogen production. green algae as a source of energy. Plant Physiology 2001;127(3):740–8.
[121] Melis A, Melnicki M. Integrated biological hydrogen production. International Journal of Hydrogen Energy 2006;31(11):1563–73.
[122] Miyake J, Mao XY, Kawamura S. Photoproduction of hydrogen from glucose by a co-culture of a photosynthetic bacterium and *Clostridium butyricum*. Journal of Fermentation Technology 1984;62(6):531–5.
[123] Daniel KJ, Incropera FP. Optical property measurements in suspensions of unicellular algae, Purdue University Technical Report, HTL 77-4; 1977.